Available online at www.sciencedirect.com

ScienceDirect

Geochimica et Cosmochimica Acta 74 (2010) 7160–7178

Geochimica et Cosmochimica Acta

www.elsevier.com/locate/gca

# Geochemical contrasts between early Cretaceous ore-bearing and ore-barren high-Mg adakites in central-eastern China: Implications for petrogenesis and Cu–Au mineralization

Sheng-Ao Liu [a,*], Shuguang Li [a,*], Yongsheng He [a], Fang Huang [b]

[a] *CAS Key Laboratory of Crust-Mantle Materials and Environments, School of Earth and Space Sciences, University of Science and Technology of China, Hefei 230026, China*

[b] *Institute of Geochemistry and Petrology, ETH Zurich, 8092 Zurich, Switzerland*

Received 3 May 2010; accepted in revised form 1 September 2010; available online 7 September 2010

**Abstract**

Adakites are commonly associated with porphyry Cu–Au ore deposits worldwide. Two groups of early Cretaceous adakites occur widely in central-eastern China but their association with mineralization contrasts sharply: adakites from the Lower Yangtze River Belt (LYRB) host one of the largest porphyry Cu–Au deposit belts in China, whereas those from the South Tan-Lu Fault (STLF), which is adjacent to the LYRB, are all ore-barren. These adakites, thus, provide a rare opportunity to explore the main factor that controls the genetic links between adakites and Cu–Au mineralization. Here we report new chronological, elemental and Sr–Nd–Pb isotopic data and present a comprehensive geochemical comparison for these two groups of adakites. At a given $SiO_2$, the STLF adakites show lower $Al_2O_3$ and higher $K_2O$, $K_2O/Na_2O$, MgO, Cr, Ni and Mg# than the LYRB adakites. These systematic differences may indicate a dry basaltic source for the STLF adakites and a water-enriched basaltic source for the LYRB adakites. The STLF adakites have high Sr/Y and $(La/Yb)_N$, which are positively correlated, and low Sr/La and Ce/Pb, while the LYRB adakites show lower $(La/Yb)_N$ but higher Sr/Y, Sr/La and Ce/Pb than the STLF adakites. Furthermore, the LYRB adakites are characterized by highly radiogenic Pb isotopic compositions with $^{206}Pb/^{204}Pb(t)$ up to 18.8, which are clearly distinct from the STLF adakites with low radiogenic Pb ($^{206}Pb/^{204}Pb(t) = 15.8–16.4$). Although the high Mg# of the two groups of adakites suggest reaction with mantle peridotites during magma ascent, the geochemical comparisons indicate that the STLF adakites were derived from partial melting of the delaminated eclogitic lower continental crust, while the LYRB adakites were derived from partial melting of the seawater-altered oceanic crust that was being subducted towards the LYRB during the early Cretaceous. The petrogenetic contrasts between these two groups of high-Mg adakites, therefore, indicate that the large-scale Cu–Au mineralization is associated with oceanic slab melting, not delamination or recycling of the ancient lower continental crust, as previously proposed.


## 1. INTRODUCTION

The Lower Yangtze River Belt (LYRB) in central-eastern China, which hosts more than 200 copper (gold)-bearing polymetallic ore deposits, makes up one of the most important metallogenic belts in China (Pan and Dong, 1999; Mao et al., 2006; Hou et al., 2007). Field investigations and chronological studies reveal that these deposits are closely associated, both spatially and temporally, with early Cretaceous intermediate to felsic calc-alkaline intrusions (e.g., Chen et al., 1991, 1993; Sun et al., 2003; Wang et al., 2006; Xie et al., 2007). Geochemical studies further show that the host intrusions exhibit some distinctive compositional characteristics resembling modern adakites in convergent plate margins (Zhang et al., 2001; Xu et al., 2002; Wang et al., 2003, 2004a, 2004b, 2006, 2007a; Xie et al., 2008; Li et al., 2009; Xie et al., 2009), as originally defined by Defant and Drummond (1990). These observations, thus, appear to

* Corresponding authors. Tel.: +86 551 3607647.
*E-mail addresses:* lsa@mail.ustc.edu.cn (S.-A. Liu), lsg@ustc.edu.cn (S. Li).

0016-7037/$ - see front matter © 2010 Elsevier Ltd. All rights reserved.
doi:10.1016/j.gca.2010.09.003

confirm a causal relationship between adakite or adakite-like magmatism and Cu–Au ore deposits, as suggested by a large number of geochemical studies of ore-bearing intrusions in porphyry districts of subduction zones around the world (e.g., Thiéblemont et al., 1997; Sajona and Maury, 1998; Oyarzun et al., 2001; Imai, 2002; Gonzalez-Partida et al., 2003; Rae et al., 2004; Borisova et al., 2006; Chiaradia et al., 2009).

Petrogenesis of the ore-bearing adakitic intrusions in the LYRB, however, has been hotly debated in the past decade (Zhang et al., 2001; Xu et al., 2002; Wang et al., 2003, 2004, 2004a, 2004b, 2006, 2007a; Hou et al., 2007; Xie et al., 2008; Li et al., 2009; Ling et al., 2009; Sun et al., 2010). Given similar bulk chemical composition but higher $^{87}Sr/^{86}Sr$ and lower $^{143}Nd/^{144}Nd$ relative to adakites from subducted oceanic slabs, these rocks were proposed to have originated from partial melting of the delaminated lower continental crust (LCC) of the Yangtze Block, followed by interaction with the mantle peridotites (Xu et al., 2002; Wang et al., 2003, 2004a, 2004b, 2006, 2007a). Consequently, delamination of the LCC has been often considered an important mechanism that could transfer Cu and Au from the mantle to the crust via the delaminated LCC-derived adakitic magmas (Wang et al., 2003, 2004a, 2004b, 2006, 2007a). Some authors, however, proposed other mechanisms to form these adakites, such as fractional crystallization of basaltic magmas possibly coupled with crustal contamination (Wang et al., 2004; Xie et al., 2008; Li et al., 2009), and partial melting of subducted oceanic crust, based on tectonic considerations (Li and Li, 2007; Ling et al., 2009; Sun et al., 2010).

Several early Cretaceous dioritic intrusions developed along the south Tan-Lu fault zone (STLF), adjacent to the LYRB in central-eastern China, also show high-Mg adakitic geochemical signatures. Derivation by partial melting of delaminated LCC of the Yangtze Block has been proposed, but these intrusions show no relationship with ore deposits (Huang et al., 2008; Zi et al., 2008; He et al., 2009). The contrasting links to mineralization between these two groups of high-Mg adakites call into question the proposed genetic link between LCC-derived magmas and Cu–Au mineralization. Because the ore-bearing and ore-barren high-Mg adakites were intruded into the Yangtze block along adjacent belts at about the same time, a comprehensive geochemical comparison can elucidate differences in their petrogenesis, and thus provide an exploration guide for Cu–Au deposits, especially in the LYRB.

In this study, we report new chronological, elemental, and Sr–Nd–Pb isotopic data for four ore-barren high-Mg adakitic intrusions from the STLF and two representative ore-bearing high-Mg adakitic intrusions from the LYRB. A detailed geochemical comparison between them is then undertaken, in order to better constrain their petrogenesis and evaluate their implications for Cu–Au mineralization.

## 2. GEOLOGICAL BACKGROUND AND SAMPLE DESCRIPTIONS

Eastern China comprises three main tectonic blocks: North China, Yangtze and Cathaysia (inset of Fig. 1). The Yangtze Block is separated from the North China Block to the north by the Triassic Dabie-Sulu orogenic belt, and from the Cathaysia block to the south by a Neoproterozoic suture. The Dabie-Sulu orogen is the largest known ultrahigh pressure metamorphic belt on the Earth. It was formed by northward subduction of the Yangtze Block beneath the North China Block in the Triassic (e.g., Li et al., 1993, 2000). The Sulu orogen is the eastern extension of the Dabie orogen, displaced ~500 km to the north by the left-lateral movement of the Tan-Lu fault during the Late Mesozoic time (inset of Fig. 1; Zhu et al., 2005). Thus, the south Tan-Lu fault (STLF) constitutes a tectonic suture between the Yangtze Block and the North China Block.

The LYRB is located in the northeast portion of the Yangtze Block in central-eastern China, referring here to the middle and lower reaches of the Yangtze River extending ~400 km from the Hubei province in the southwest to the Jiangsu province in the northeast (Fig. 1). This belt makes up one of the most important metallogenic belts in China and comprises seven major deposit districts from southwest to northeast along the Yangtze River (Fig. 1). The ore deposits throughout the LYRB mainly consist of skarn, porphyry and strata-bound polymetallic (Cu, Au, Fe, Mo, Zn, Pb, and Ag) deposits (Xing, 1999). Dating of the ore-forming minerals indicates that they formed in the early Cretaceous (143–134 Ma) and the skarn, porphyry and strata-bound mineralization were contemporaneous (Sun et al., 2003; Mao et al., 2006; Xie et al., 2007). The host intrusions are mainly dioritic (adakite-like) rocks and have emplacement ages identical to the formation ages of associated deposits (~143–134 Ma; Chen et al., 1991; Sun et al., 2003; Wang et al., 2003, 2004a, 2006, 2007a; Xie et al., 2009; Li et al., 2009), indicative of spatial and temporal association between host rocks and ore deposits. In this study, nine samples from two representative intrusions (Tongguanshan and Yueshan; Fig. 1) were selected for geochemical studies. Samples are mainly fresh quartz diorite, with plagioclase (30–40%), quartz (20–25%), amphibole (15–25%), K-feldspar (10–15%), biotite (5–10%), and minor zircon and sphene.

The STLF refers here to the areas adjacent to the south segment of the Tan-Lu fault zone in the eastern Yangtze Block and in the eastern margin of the Dabie orogen, which is adjacent to the LYRB on the north (Fig. 1). The early Cretaceous dioritic to granodioritic intrusions located in the eastern margin of the Dabie orogen, southern section of the STLF, have been identified as high-Mg adakitic rocks, e.g., Chituling, Guanghui, and Meichuan intrusions (Huang et al., 2008; He et al., 2009; Liu et al. 2010) (Fig. 1). In the northern section of the STLF, the early Cretaceous Guandian (Zi et al., 2008), Wawuliu, and Wawuxue intrusions (Niu et al., 2002) were also categorized into high-Mg adakitic rocks (Fig. 1). In this study, we selected 16 samples from four intrusions in the northern section of the STLF in the eastern Yangtze Block, i.e., Fangjiangzhuang, Damaocun, Xiaolizhuang and Qiaotouji (Fig. 1). These localities occur as small intrusions having an exposure area of about 8, 4, 2 and 10 $km^2$, respectively. Samples consist mainly of monzonite and quartz monzonite, with plagioclase (25–40%), amphibole (20–30%), K-feldspar (15–25%), quartz (10–20%), biotite (5–10%), and minor

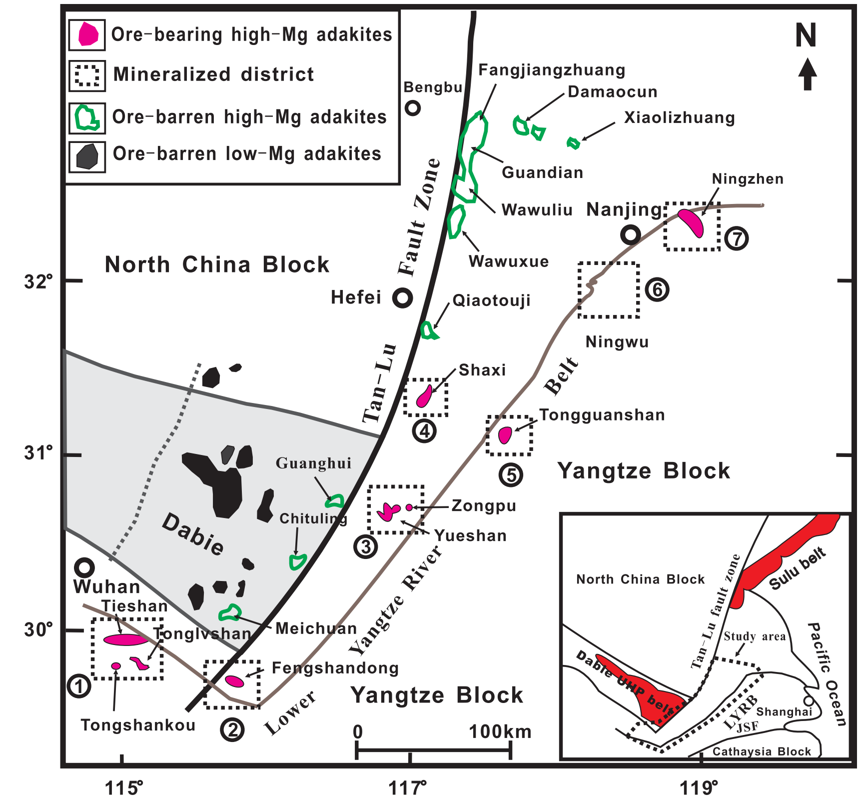


Fig. 1. Simplified geologic map of the central-eastern China, showing the spatial distribution of early Cretaceous adakites from the Lower Yangtze River Belt (LYRB) and areas along the south segment of the Tan-Lu fault zone (STLF). The seven major mineralization districts in the LYRB are also shown: ①, Edong; ②, Jiurui; ③, Anqing; ④, Luzong; ⑤, Tongling; ⑥, Ningwu; ⑦, Anjishan. JSF in the inset denotes the Jiangshan-Shaoxing fault which represents the geological boundary between the Yangtze and Cathaysia blocks.

zircon and sphene. These intrusions are not spatially associated with mafic igneous rocks, and all are ore-barren.

## 3. ANALYTICAL METHODS

Zircon grains were separated from the four investigated STLF intrusions using magnetic and heavy liquid separation methods and finally by hand-picking under a binocular microscope. Approximately 100–200 grains for each sample were mounted in an epoxy resin disc together with the zircon standard TEMORA (Black et al., 2004). Prior to U–Th–Pb isotope analysis, all grains were photographed under transmitted- and reflected-light, and subsequently examined using the cathodoluminescence (CL) image technique to reveal the internal structures of individual zircon grains. Isotopic analysis was performed using a Cameca-IMS 1280 in the SIMS center of the Institute of Geology and Geophysics, Chinese Academy of Science, following the procedure outlined in Li et al. (2010). The spot size of an ion beam was ~30 μm. Measured isotopic ratios were corrected for common Pb using the measured non-radiogenic $^{204}$Pb. U–Pb ages were calculated using the ISOPLOT program of Ludwig (2001).

Major elements for the STLF samples were analyzed by wet-chemistry methods at the Langfang laboratory of Regional Geological Exploration Bureau of Hebei Province, China. Losses of ignition (LOI) were determined by gravimetric methods. Analytical uncertainties for the majority of major elements were better than 1%. Major elements for the LYRB samples were analyzed in Göttingen using a PANalytical AXIOS advanced sequential X-ray spectrometer. The long-term analytical precision was better than 1–2%. For trace element determination, whole-rock powder (~50 mg) was dissolved in a mixture of $HF + HNO_3$ at 190 °C using Parr bombs for ~72 h. Dissolved samples were diluted to 50 ml using 1% $HNO_3$ before analyses. Analyses were accomplished using an inductively coupled plasma mass spectrometer (ICP-MS) at the University of Science and Technology of China. Detailed analytical procedures were described in Hou and Wang (2007). Reproducibility was better than 5% for elements with concentrations >10 ppm and less than 10% for those <10 ppm.

The Rb–Sr and Sm–Nd concentrations and isotopic ratios were determined by isotope dilution methods. Isotopic measurement was performed on a Finnigan MAT-262 thermal ionization mass spectrometer (TIMS) at the Institute of Geology and Geophysics, Chinese Academy of Sciences. The mass fractionation corrections for Sr and Nd isotopic ratios were based on $^{86}Sr/^{88}Sr = 0.1194$ and $^{146}Nd/^{144}Nd = 0.7219$, respectively. Detailed analytical procedures were

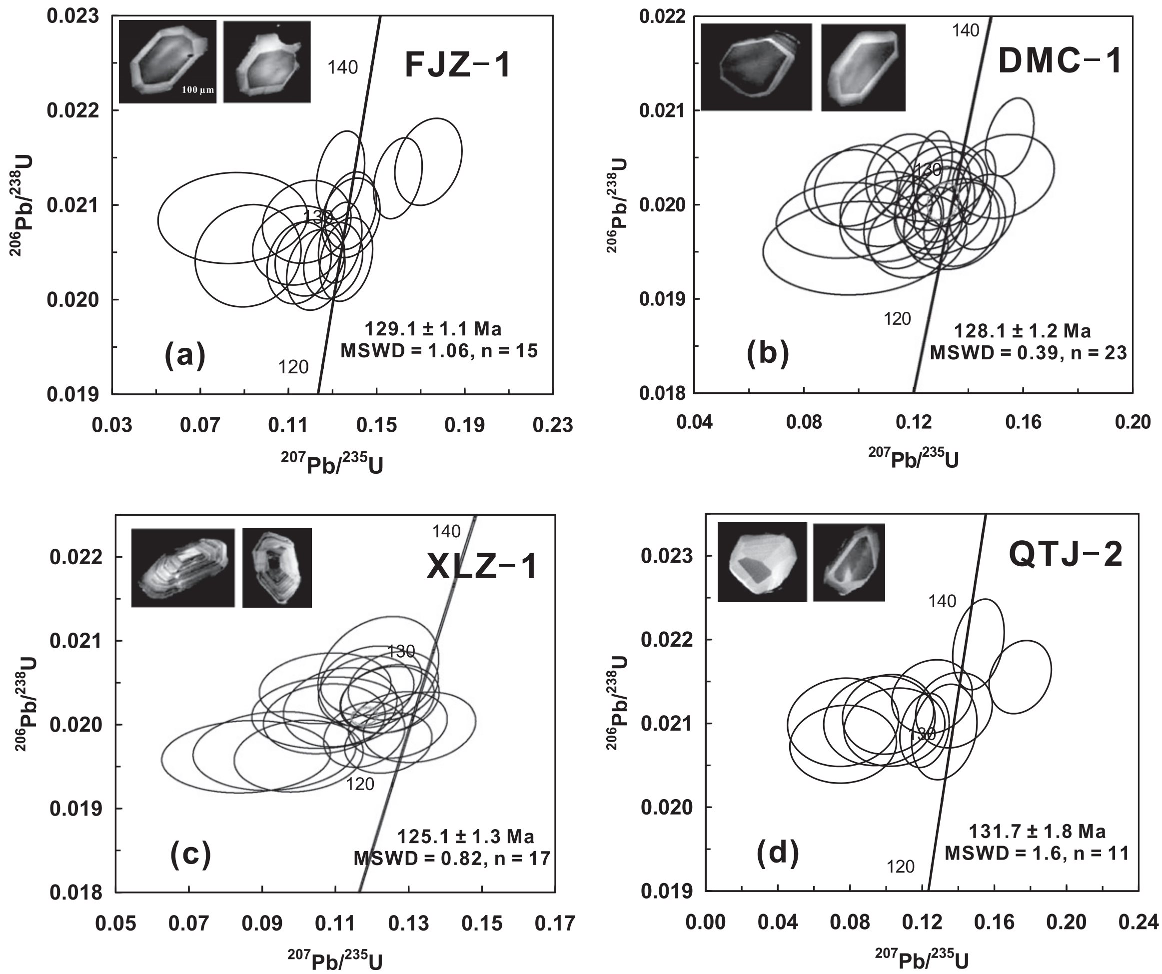


Fig. 2. Zircon U–Pb concordia diagrams and CL images of representative zircon grains for (a) Fangjiangzhuang, (b) Damaochun, (c) Xiaolizhuang, and (d) Qiaotouji intrusions. Data are from Supplementary Table A1. The uncertainties of ages are reported at 1σ.

described in Chen et al. (2002b). Analyses of standards during the period of analysis were as follows: NBS987 of $^{87}Sr/^{86}Sr = 0.710248 \pm 12$ (2σ); and Jndi-1 of $^{143}Nd/^{144}Nd = 0.512112 \pm 12$ (2σ). For Pb isotopic determination, fresh plagioclase of the LYRB samples was analyzed for common Pb and the STLF samples were analyzed in whole-rock powder. Samples were dissolved in concentrated HF, and Pb was purified by cation-exchange technique following the procedure described by He et al. (2005). Isotopic ratios were measured with a multi-collector inductively coupled plasma mass spectrometer (MC-ICP-MS) at the Institute of Geology, Chinese Academy of Geological Sciences. Thallium was added as an internal standard to determine thermal fractionation. Long-term analysis of the NBS981 standard yielded $^{206}Pb/^{204}Pb = 16.940 \pm 0.010$ (±2σ), $^{207}Pb/^{204}Pb = 15.498 \pm 0.009$, and $^{208}Pb/^{204}Pb = 36.716 \pm 0.023$, respectively.

## 4. RESULTS

### 4.1. Zircon U–Pb dating

Zircons from the four investigated STLF intrusions are generally prismatic, colorless, transparent, and euhedral. Most zircon grains display oscillatory zoning as shown in CL images with Th/U values of 0.6–1.4 (Supplementary material Table A1; Fig. 2), typical of magmatic zircons. Analyses of >15 spots yielded concordant U–Pb ages, with weighted mean $^{206}Pb/^{238}U$ ages of 129.1 ± 1.1 Ma, 128.1 ± 1.2 Ma, and 125.1 ± 1.3 Ma for the Fangjiangzhuang, Damaochun and Xiaolizhuang intrusions, respectively (Fig. 2a–c). Analyses of 11 spots of zircons from the Qiaotouji intrusion yielded large uncertainties on $^{207}Pb/^{235}U$ ages (Fig. 2d), which is probably due to low accumulated amounts of radiogenic $^{207}Pb$ in these young (Phanerozoic; see below), low-U zircons (23–65 ppm; Supplementary Table A1). Nevertheless, all analyses gave homogeneous $^{206}Pb/^{238}U$ ages with a weighted mean of 131.7 ± 1.8 Ma (Fig. 2d), which is considered as the crystallization time of the Qiaotouji intrusion. Zircon dating results and CL images did not reveal any inherited zircons in any of the four intrusions.

In summary, zircon U–Pb dating results of the four investigated STLF intrusions are comparable to those of previously reported high-Mg adakitic intrusions from the STLF (Huang et al., 2008; Zi et al., 2008; He et al., 2009), which have zircon U–Pb ages of 132–125 Ma with a peak at 132–130 Ma. There appears to be a geographic

Table 1
Major (wt.%) and trace element (ppm) concentrations of adakitic intrusions from the STLF and the LYRB reported in this study.

| Location | STLF | | | | | | | | | | | | | | | | LYRB | | | | | | | | |
|---|---|---|---|---|---|---|---|---|---|---|---|---|---|---|---|---|---|---|---|---|---|---|---|---|---|
| Sample | DMC | DMC | DMC | DMC | XLZ | XLZ | XLZ | XLZ | FJZ | FJZ | FJZ | FJZ | QTJ | QTJ | QTJ | QTJ | YS | YS | YS | YS | YS | YS | TGS | TGS | TGS |
| No. | −1 | −2 | −5 | −7 | −1 | −2 | −4 | −6 | −1 | −2 | −4 | −6 | −2 | −3 | −4 | −5 | −1 | −2 | −3 | −4 | −5 | −7−2 | −2 | −3 | −7 |
| $SiO_2$ | 58.9 | 62.0 | 62.5 | 62.6 | 65.9 | 66.0 | 66.1 | 66.1 | 60.4 | 61.7 | 60.5 | 60.3 | 56.2 | 63.4 | 62.5 | 62.2 | 59.8 | 57.4 | 59.3 | 57.5 | 59.0 | 57.8 | 62.8 | 63.78 | 61.6 |
| $TiO_2$ | 0.81 | 0.72 | 0.69 | 0.68 | 0.52 | 0.49 | 0.43 | 0.47 | 0.65 | 0.68 | 0.75 | 0.66 | 0.62 | 0.55 | 0.59 | 0.66 | 0.62 | 0.78 | 0.68 | 0.77 | 0.69 | 0.77 | 0.54 | 0.55 | 0.57 |
| $Al_2O_3$ | 15.6 | 15.2 | 15.1 | 15.2 | 15.1 | 15.1 | 15.2 | 15.3 | 14.6 | 14.6 | 14.5 | 14.7 | 15.6 | 14.4 | 14.8 | 14.0 | 16.2 | 16.6 | 16.2 | 16.7 | 16.2 | 16.6 | 16.5 | 16.5 | 16.4 |
| $TFe_2O_3$ | 6.61 | 5.66 | 5.42 | 5.28 | 3.58 | 3.46 | 3.30 | 3.39 | 5.94 | 5.59 | 5.91 | 6.04 | 5.91 | 4.64 | 5.14 | 5.53 | 4.98 | 6.13 | 5.24 | 6.05 | 5.33 | 5.91 | 2.36 | 4.4 | 4.55 |
| MnO | 0.11 | 0.09 | 0.09 | 0.09 | 0.06 | 0.06 | 0.05 | 0.05 | 0.10 | 0.09 | 0.09 | 0.10 | 0.10 | 0.08 | 0.08 | 0.09 | 0.09 | 0.10 | 0.09 | 0.10 | 0.09 | 0.10 | 0.07 | 0.07 | 0.06 |
| MgO | 3.45 | 3.02 | 2.74 | 3.07 | 1.97 | 2.30 | 2.21 | 2.33 | 4.57 | 3.85 | 4.17 | 4.83 | 6.05 | 3.86 | 3.93 | 4.28 | 3.0 | 3.21 | 2.87 | 3.39 | 2.47 | 3.43 | 1.43 | 1.47 | 1.63 |
| CaO | 4.79 | 4.03 | 3.93 | 3.57 | 3.90 | 3.65 | 3.43 | 3.26 | 5.21 | 4.69 | 5.13 | 4.89 | 4.29 | 3.77 | 4.27 | 4.27 | 5.09 | 5.77 | 4.88 | 5.71 | 4.69 | 5.65 | 7.67 | 4.65 | 4.64 |
| $Na_2O$ | 4.09 | 4.05 | 4.05 | 4.13 | 4.32 | 4.17 | 4.44 | 4.40 | 3.94 | 3.98 | 3.86 | 3.86 | 4.55 | 3.92 | 4.15 | 3.85 | 4.66 | 5.0 | 4.75 | 4.94 | 4.75 | 4.93 | 5.29 | 4.83 | 4.74 |
| $K_2O$ | 3.48 | 4.14 | 4.14 | 4.17 | 3.62 | 3.84 | 3.37 | 3.48 | 3.26 | 3.81 | 3.40 | 3.51 | 3.70 | 3.96 | 3.44 | 3.70 | 2.66 | 2.91 | 3.19 | 2.88 | 3.3 | 2.98 | 0.53 | 2.68 | 2.76 |
| $P_2O_5$ | 0.41 | 0.34 | 0.32 | 0.33 | 0.20 | 0.19 | 0.18 | 0.37 | 0.35 | 0.36 | 0.39 | 0.35 | 0.35 | 0.25 | 0.28 | 0.29 | 0.34 | 0.47 | 0.38 | 0.44 | 0.38 | 0.46 | 0.25 | 0.26 | 0.27 |
| $H_2O$ | 0.42 | 0.33 | 0.39 | 0.46 | 0.18 | 0.27 | 0.24 | 0.16 | 0.59 | 0.52 | 0.34 | 0.5 | 1.62 | 0.44 | 0.43 | 0.45 | nd | nd | nd | nd | nd | nd | nd | nd | nd |
| LOI | 0.95 | 0.89 | 0.84 | 0.92 | 0.83 | 0.85 | 1.12 | 0.81 | 1.00 | 0.77 | 0.94 | 1.13 | 2.43 | 0.87 | 0.81 | 1.03 | nd | nd | nd | nd | nd | nd | nd | nd | nd |
| $\sum$ | 98.8 | 99.7 | 99.5 | 99.7 | 99.8 | 99.9 | 99.7 | 99.8 | 99.6 | 99.8 | 99.3 | 99.9 | 99.4 | 99.4 | 99.6 | 99.5 | 97.4 | 98.3 | 97.6 | 98.5 | 97.0 | 98.6 | 97.5 | 99.2 | 97.2 |
| $K_2O/Na_2O$ | 0.85 | 1.02 | 1.02 | 1.01 | 0.84 | 0.92 | 0.76 | 0.79 | 0.83 | 0.96 | 0.88 | 0.91 | 0.81 | 1.01 | 0.83 | 0.96 | 0.57 | 0.58 | 0.67 | 0.58 | 0.69 | 0.60 | 0.10 | 0.55 | 0.58 |
| Mg# | 51 | 52 | 50 | 54 | 52 | 57 | 57 | 58 | 61 | 58 | 59 | 62 | 67 | 62 | 60 | 61 | 55 | 51 | 52 | 53 | 48 | 54 | 55 | 40 | 42 |
| Ba | 1284 | 1209 | 1148 | 1143 | 1211 | 1670 | 1201 | 1257 | 1758 | 1725 | 1906 | 1912 | 1983 | 1775 | 1563 | 1673 | 1127 | 1167 | 1110 | 1195 | 1196 | 1191 | 1322 | 1222 | 1089 |
| Rb | 111.0 | 134.0 | 137.0 | 139.0 | 80.0 | 92.3 | 81.7 | 83.4 | 71.4 | 77.9 | 73.0 | 74.6 | 88.3 | 77.6 | 69.8 | 74.9 | 60.0 | 48.0 | 61.0 | 49.0 | 63.0 | 51.0 | 50.1 | 61.0 | 73.0 |
| Sr | 949 | 794 | 769 | 775 | 743 | 782 | 820 | 807 | 911 | 780 | 921 | 939 | 1040 | 816 | 876 | 793 | 1487 | 1763 | 1498 | 1702 | 1445 | 1659 | 1138 | 1121 | 1101 |
| Y | 17.1 | 17.7 | 18.1 | 17.4 | 11.1 | 10.4 | 10.1 | 10.7 | 15.5 | 15.9 | 15.4 | 16.5 | 14.3 | 13.8 | 15.0 | 16.5 | 12.2 | 15.3 | 14.8 | 15.3 | 16.4 | 14.8 | 14.9 | 15.3 | 16.2 |
| Sc | 14.4 | 12.9 | 11.9 | 11 | 6.91 | 7.4 | 6.84 | 7.17 | 14.1 | 13.6 | 14.1 | 15.4 | 14.9 | 11 | 11.7 | 13.1 | nd | nd | nd | nd | nd | nd | nd | nd | nd |
| Co | 20.5 | 16.5 | 15.7 | 15.5 | 10.8 | 10.8 | 10.1 | 10.3 | 20.2 | 15.4 | 19.9 | 21.3 | 24.4 | 16.0 | 18.5 | 19.8 | 15.0 | 20.0 | 17.0 | 18.0 | 14.0 | 18.0 | 5.0 | 8.0 | 9.0 |
| Cr | 95.2 | 49.4 | 50.9 | 48.4 | 59.3 | 50.7 | 66.1 | 46.2 | 172 | 154 | 163 | 185 | 263 | 151 | 166 | 176 | 43 | 25 | 31 | 38 | 19 | 33 | 12 | 15 | 19 |
| Ni | 49.8 | 28.9 | 27.9 | 25.7 | 32.2 | 29.3 | 45.2 | 25.9 | 67.3 | 56.5 | 65.1 | 72.0 | 121 | 64.6 | 78 | 80.1 | 22 | 18 | 17 | 21 | 12 | 22 | 12 | 10 | 10 |
| Zr | 30.1 | 62.8 | 296.0 | 212.0 | 158.0 | 147.0 | 166.0 | 148.0 | 164.0 | 139.0 | 183.0 | 220.0 | 162 | 134 | 177 | 163 | 144 | 182 | 158 | 131 | 170 | 180 | 195 | 189 | 189 |
| Nb | 11.5 | 14.4 | 13.6 | 13.3 | 10.1 | 8.6 | 8.8 | 10.1 | 8.9 | 8.5 | 9.0 | 9.3 | 7.9 | 9.4 | 10.4 | 11.6 | 3.7 | 5.1 | 6.8 | 4.3 | 8.1 | 4.3 | 11.2 | 10.1 | 11.6 |
| Th | 11.4 | 13.4 | 13 | 12.6 | 6.08 | 6.1 | 7.06 | 7.66 | 7.29 | 7.73 | 7.94 | 8.57 | 4.85 | 3.1 | 8.3 | 8.3 | 8.9 | 8.0 | 10.0 | 7.1 | 11.3 | 8.2 | 7.7 | 0.9 | 6.0 |
| Pb | 24.5 | 24.7 | 26.1 | 24.2 | 16.6 | 18 | 19 | 18.4 | 21.7 | 21.7 | 22.5 | 24.8 | 20.8 | 24.7 | 14.9 | 16.6 | 15 | 14 | 17 | 15 | 15 | 18 | 4 | 7 | 10 |
| V | 128 | 109 | 120 | 107 | 67 | 73 | 68 | 69 | 130 | 107 | 134 | 141 | 128 | 99 | 106 | 122 | 112 | 146 | 132 | 153 | 124 | 155 | 59 | 64 | 65 |
| Hf | 1.1 | 1.7 | 6.4 | 4.6 | 3.5 | 3.3 | 3.7 | 3.4 | 3.7 | 3.2 | 4.2 | 5.0 | 3.7 | 3.2 | 4.1 | 3.9 | 3.5 | 4.7 | 4.5 | 3.2 | 4 | 4.2 | 5.1 | 4.9 | 4.8 |
| Cs | 5.6 | 5.7 | 6.3 | 6.0 | 1.2 | 1.3 | 1.4 | 1.4 | 3.1 | 3.0 | 2.8 | 2.7 | 1.4 | 1.53 | 0.8 | 0.82 | nd | nd | nd | nd | nd | nd | nd | nd | Nd |
| Ta | 0.61 | 0.77 | 0.74 | 0.68 | 0.76 | 0.63 | 0.64 | 0.79 | 0.54 | 0.52 | 0.57 | 0.56 | 0.36 | 0.54 | 0.64 | 0.75 | nd | nd | nd | nd | nd | nd | nd | nd | Nd |
| U | 3.3 | 3.2 | 2.9 | 2.7 | 1.5 | 1.6 | 1.9 | 2.1 | 1.9 | 2.0 | 1.9 | 1.8 | 1.7 | 1.7 | 5.6 | 2.4 | 2.4 | 2.1 | 2.6 | 1.9 | 3 | 2.2 | 2 | 0.3 | 1.5 |
| La | 45.1 | 53.3 | 49.9 | 51.9 | 33.3 | 31.3 | 30.2 | 34.7 | 37.2 | 37.0 | 36.5 | 38.4 | 42.1 | 26.4 | 37.9 | 34.2 | 33 | 45 | 42 | 39 | 51 | 44 | 30 | 36 | 34 |
| Ce | 86.7 | 101.0 | 94.3 | 95.6 | 57.4 | 53.8 | 52.7 | 59.4 | 68.5 | 64.8 | 66.9 | 70.7 | 79.4 | 53.6 | 70.1 | 67.7 | 67.0 | 93.0 | 85.0 | 84.0 | 98.0 | 85.0 | 63.0 | 68.0 | 70.0 |
| Pr | 9.7 | 11.1 | 10.4 | 10.4 | 6.0 | 5.6 | 5.5 | 6.1 | 7.6 | 7.6 | 7.5 | 7.9 | 9.0 | 6.4 | 7.8 | 7.9 | nd | nd | nd | nd | nd | nd | nd | nd | Nd |
| Nd | 38.1 | 42.1 | 39.2 | 38.9 | 21.5 | 20.3 | 19.8 | 21.5 | 29.4 | 29.3 | 28.8 | 30.9 | 34.9 | 25.2 | 29.5 | 31.0 | 30.8 | 41.9 | 38 | 40.5 | 42.8 | 39.8 | 28 | 30.1 | 34.2 |
| Sm | 6.8 | 7.1 | 6.6 | 6.5 | 3.4 | 3.2 | 3.1 | 3.4 | 4.9 | 4.9 | 4.9 | 5.2 | 5.8 | 4.4 | 4.9 | 5.4 | 6.1 | 8.6 | 7.8 | 8.2 | 8.5 | 8.3 | 6.0 | 6.4 | 7.4 |
| Eu | 1.9 | 1.7 | 1.5 | 1.5 | 0.95 | 0.97 | 0.95 | 0.96 | 1.4 | 1.3 | 1.4 | 1.5 | 1.6 | 1.2 | 1.4 | 1.4 | nd | nd | nd | nd | nd | nd | nd | nd | nd |

| | | | | | | | | | | | | | | | | | | | | | | | | | |
|---|---|---|---|---|---|---|---|---|---|---|---|---|---|---|---|---|---|---|---|---|---|---|---|---|---|
| Gd | 5.13 | 5.09 | 4.71 | 4.59 | 2.48 | 2.25 | 2.18 | 2.27 | 3.63 | 3.51 | 3.56 | 3.91 | 3.9 | 3.16 | 3.50 | 3.81 | nd | nd | nd | nd | nd | nd | nd | nd | nd |
| Tb | 0.63 | 0.65 | 0.61 | 0.58 | 0.33 | 0.3 | 0.3 | 0.32 | 0.48 | 0.48 | 0.48 | 0.52 | 0.49 | 0.43 | 0.46 | 0.52 | nd | nd | nd | nd | nd | nd | nd | nd | nd |
| Dy | 3.52 | 3.47 | 3.6 | 3.42 | 1.97 | 1.93 | 1.87 | 1.98 | 2.95 | 3.04 | 2.98 | 3.24 | 2.87 | 2.68 | 2.89 | 3.22 | nd | nd | nd | nd | nd | nd | nd | nd | nd |
| Ho | 0.61 | 0.61 | 0.62 | 0.59 | 0.38 | 0.35 | 0.34 | 0.35 | 0.53 | 0.53 | 0.52 | 0.57 | 0.49 | 0.46 | 0.52 | 0.55 | nd | nd | nd | nd | nd | nd | nd | nd | nd |
| Er | 1.44 | 1.51 | 1.62 | 1.42 | 0.98 | 0.94 | 0.93 | 0.97 | 1.32 | 1.44 | 1.42 | 1.54 | 1.17 | 1.25 | 1.26 | 1.49 | nd | nd | nd | nd | nd | nd | nd | nd | nd |
| Tm | 0.22 | 0.23 | 0.21 | 0.21 | 0.15 | 0.13 | 0.13 | 0.13 | 0.19 | 0.2 | 0.19 | 0.21 | 0.17 | 0.17 | 0.19 | 0.20 | nd | nd | nd | nd | nd | nd | nd | nd | nd |
| Yb | 1.37 | 1.48 | 1.45 | 1.42 | 1.07 | 0.91 | 0.90 | 0.97 | 1.36 | 1.35 | 1.33 | 1.43 | 1.13 | 1.14 | 1.31 | 1.38 | 1.31 | 1.50 | 1.30 | 2.0 | 1.83 | 1.40 | 1.52 | 0.70 | 1.90 |
| Lu | 0.21 | 0.22 | 0.21 | 0.2 | 0.15 | 0.14 | 0.14 | 0.14 | 0.19 | 0.2 | 0.19 | 0.21 | 0.15 | 0.17 | 0.18 | 0.20 | nd | nd | nd | nd | nd | nd | nd | nd | nd |
| Eu/Eu* | 0.93 | 0.72 | 0.70 | 0.74 | 0.99 | 1.23 | 1.23 | 1.13 | 1.04 | 0.97 | 1.07 | 1.03 | 0.93 | 1.03 | 0.99 | 0.88 | nd | nd | nd | nd | nd | nd | nd | nd | nd |
| Sr/Y | 55.5 | 44.9 | 42.5 | 44.5 | 66.9 | 75.2 | 81.2 | 75.4 | 58.8 | 49.1 | 59.8 | 56.9 | 72.7 | 59.1 | 58.4 | 48.1 | 121.9 | 115.2 | 101.2 | 111.2 | 88.1 | 112.1 | 76.4 | 73.3 | 68.0 |
| $(La/Yb)_N$ | 23.6 | 25.8 | 24.7 | 26.2 | 22.3 | 24.7 | 24.1 | 25.7 | 19.6 | 19.7 | 19.7 | 19.3 | 26.7 | 16.6 | 20.8 | 17.8 | 18.2 | 21.5 | 23.2 | 14.0 | 20.3 | 22.5 | 14.3 | 36.9 | 12.8 |
| Ce/Pb | 3.54 | 4.09 | 3.61 | 3.95 | 3.46 | 2.99 | 2.77 | 3.23 | 3.16 | 2.99 | 2.97 | 2.85 | 3.82 | 2.2 | 4.7 | 4.1 | 4.5 | 6.6 | 5.0 | 5.6 | 6.5 | 4.7 | 15.8 | 9.7 | 7.0 |

Mg# = 100 × molar Mg/(Mg + Total Fe); Eu/Eu* = $Eu_N/(Sm_N \times Gd_N)1/2$, N denotes the chondrite normalization (Sun and McDonough, 1989).
nd = not determined.

age structure among these intrusions, i.e., intrusions further apart from the Tan-Lu fault (e.g., Damaochun and Xiaolizhuang) are younger than those located closer to the Tan-Lu fault (Fig. 1). Notably, ore-barren intrusions from the STLF are slightly younger than the ore-bearing intrusions from the LYRB.

### 4.2. Major and trace element compositions

The intrusions from the STLF studied here are dioritic with $SiO_2$ contents ranging from 56.2 to 66.1 wt.% (Table 1). They can be classified as monzonite and quartz monzonite (Fig. 3) and belong to the sub-alkaline series based on the classification of Irvine and Baragar (1971). They have $Al_2O_3$ contents of 14.0–15.6 wt.% and $K_2O/Na_2O$ ranging from 0.81 to 1.02. These intrusions are characterized by prominent enrichment in light rare earth elements (LREE) relative to heavy REE (HREE) with $(La/Yb)_N$ ranging from 16.6 to 26.7 (Fig. 4). They are enriched in large ion lithophile elements (LILEs) and depleted in high field strength elements (HFSEs), with pronounced negative anomalies of Nb, Ta, and Ti and positive anomalies of Pb (Fig. 4). The high Sr (743–1040 ppm), low Y (10.1–18.1 ppm) and HREE contents (e.g., Yb = 0.90–1.48 ppm) and resultant high Sr/Y (42.5–81.2) and $(La/Yb)_N$ jointly indicate that the SLTF intrusions studied here can be classified as adakitic rocks (Fig. 5), as defined by Defant and Drummond (1990). In addition, they have relatively high Mg# (50–67), MgO (1.97–6.05 wt.%), Cr (46–263 ppm), and Ni (26–121 ppm) contents (Table 1).

Samples from the LYRB studied here exhibit smaller variations in major element composition than the STLF samples (Table 1). They can be mainly grouped as diorite and monzonite and belong to the alkaline or sub-alkaline series (Fig. 3). They have relatively high $Al_2O_3$ contents of 16.2–16.7 wt.% and low $K_2O/Na_2O$ of 0.10–0.69. All samples exhibit high Sr (1101–1763 ppm), low Y (12.2–16.4 ppm) and Yb (0.7–1.8 ppm) contents and high Sr/Y (73.3–121.9) and $(La/Yb)_N$ (12.8–23.2; one sample = 36.9; Table 1), which fall in the adakite field (Fig. 5). These intrusions have moderately high Mg# (40–55) and MgO (1.43–3.43 wt.%), Cr (12–43 ppm) and Ni (10–22 ppm) contents (Table 1).

### 4.3. Sr–Nd–Pb isotopic compositions

The STLF intrusions studied here have initial Sr and Nd isotope compositions with $(^{87}Sr/^{86}Sr)_i$ = 0.70569 to 0.70696 and $\varepsilon_{Nd}(t)$ = –17.4 to –11.4 (Table 2). Samples from the Tongguanshan intrusion in the LYRB have $(^{87}Sr/^{86}Sr)_i$ from 0.70720 to 0.70730 and $\varepsilon_{Nd}(t)$ from –10.8 to –11.4; samples from the Yueshan intrusion show slightly lower $(^{87}Sr/^{86}Sr)_i$ (0.70648–0.70670) and higher $\varepsilon_{Nd}(t)$ (–7.1 to –8.1), comparable to previously reported data for the Yueshan intrusion (($^{87}Sr/^{86}Sr)_i$ = 0.7064–0.7066; $\varepsilon_{Nd}(t)$ = –6.6 to –8.7; Wang et al., 2004a).

In this study we report new Pb isotopic data for intrusions from both the STLF and LYRB (Table 3). Samples from the STLF are characterized by low radiogenic Pb isotopes with $^{206}Pb/^{204}Pb(t)$ = 16.26–16.38, $^{207}Pb/^{204}Pb(t)$ = 15.34–15.40,

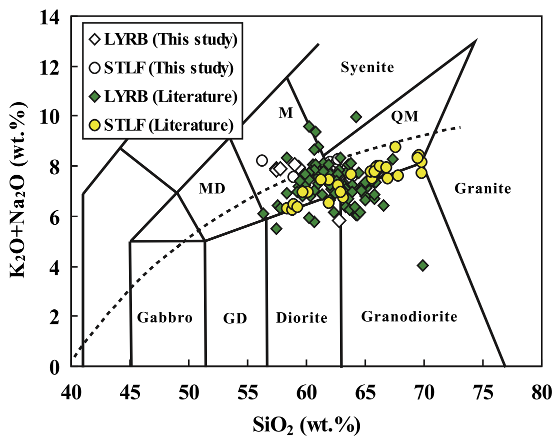


Fig. 3. Total alkalis ($Na_2O + K_2O$) versus $SiO_2$ diagram for investigated intrusions from the LYRB and STLF. The dashed line represents the division between alkaline and sub-alkaline (Irvine and Baragar, 1971). GD: granitic diorite; MD: monzonitic diorite; M: monzonite; QM: quartz monzonite. Data are from this study (Table 1) and the literature (Supplementary Tables A2 and A3; Niu et al., 2002; Xu et al., 2002; Wang et al., 2001, 2002, 2003, 2004a, 2004b, 2006, 2007a; Huang et al., 2008; Zi et al., 2008; He et al., 2009; Li et al., 2009).

and $^{208}Pb/^{204}Pb(t) = 36.56–36.90$, which are similar to previously reported data of the Chituling high-Mg adakitic intrusions from the STLF ($^{206}Pb/^{204}Pb(t) = 15.81–16.29$, $^{207}Pb/^{204}Pb(t) = 15.17–15.30$ and $^{208}Pb/^{204}Pb(t) = 36.62–37.35$; Huang et al., 2008). Plagioclases from the Yueshan and Tongguanshan samples in the LYRB display higher radiogenic Pb with $^{206}Pb/^{204}Pb = 17.74–17.90$, $^{207}Pb/^{204}Pb = 15.48–15.55$, and $^{208}Pb/^{204}Pb = 37.94–38.06$.

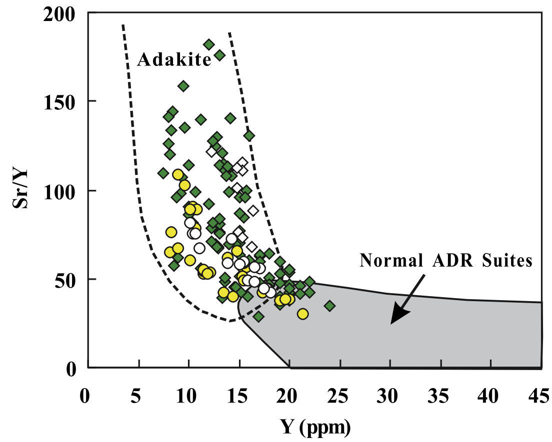


Fig. 5. Sr/Y versus Y classification diagram for investigated intrusions from the LYRB and STLF (after Defant and Drummond, 1990). Data sources are the same as in Fig. 3.

## 5. DISCUSSION

The chemical and isotopic data for the STLF and LYRB intrusions reported in this study and in the literature are compiled here for discussion. Generally, these two groups of intrusions have a similar $SiO_2$ concentration range (Fig. 3) with adakitic signature that extends throughout the entire compositional range (Fig. 5). However, a detailed geochemical comparison between them reveals remarkable differences (Table 4), suggesting that they have distinct petrogenesis, although they were almost contemporaneously intruded into the Yangtze Block. The geochemical differences and the relevant interpretations for these differences,

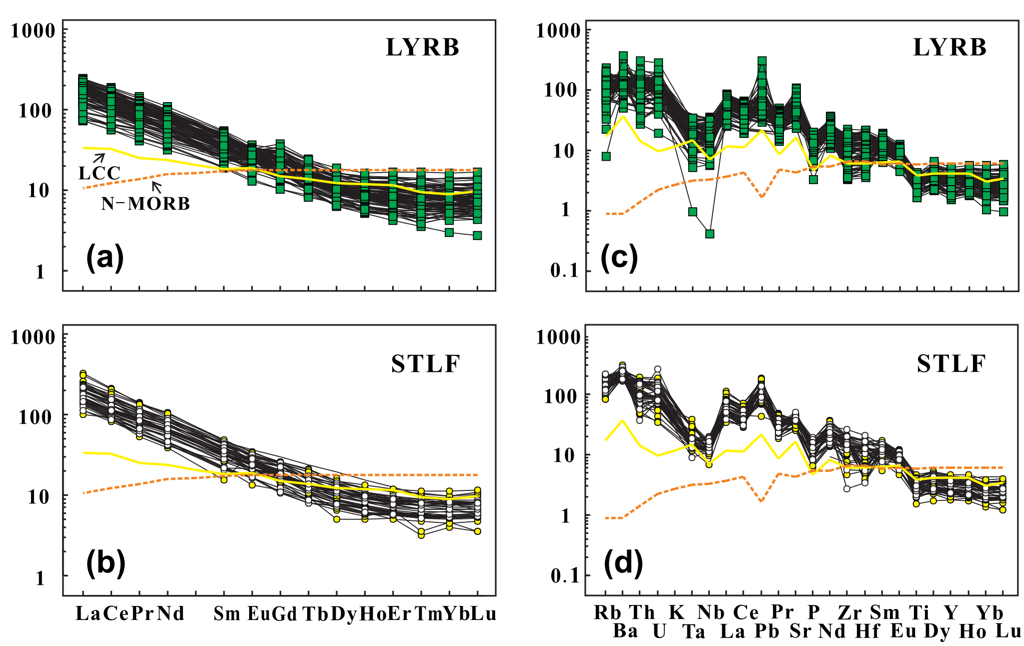


Fig. 4. Chondrite normalized rare earth element patterns (a and b) and primitive mantle normalized trace element patterns (c and d) for investigated intrusions from the LYRB and STLF. The normalizing values are from Sun and McDonough (1989). LCC is from Rudnick and Gao (2003) and N-MORB is from Sun and McDonough (1989). Data sources for the LYRB and STLF samples are the same as in Fig. 3.

Table 2
Whole-rock Sr and Nd isotopic data of adakitic intrusions from the STLF and the LYRB reported in this study.

| Sample No. | Rb ppm | Sr ppm | $^{87}Rb/^{86}Sr$ | $^{87}Sr/^{86}Sr$ | $2\sigma$ | $(^{87}Sr/^{86}Sr)_i$ | Sm ppm | Nd ppm | $^{147}Sm/^{144}Nd$ | $^{143}Nd/^{144}Nd$ | $2\sigma$ | $\varepsilon_{Nd}(t)$ |
|---|---|---|---|---|---|---|---|---|---|---|---|---|
| *STLF* | | | | | | | | | | | | |
| DMC-1 | 103.7 | 942.9 | 0.3183 | 0.70730 | 12 | 0.70671 | 6.394 | 35.79 | 0.1080 | 0.51184 | 11 | −14.2 |
| DMC-2 | 126.1 | 800.2 | 0.4561 | 0.70770 | 11 | 0.70671 | 6.430 | 37.90 | 0.1026 | 0.51180 | 10 | −14.8 |
| DMC-5 | 122.9 | 768.1 | 0.4631 | 0.70772 | 10 | 0.70686 | 6.345 | 36.74 | 0.1044 | 0.51182 | 11 | −14.5 |
| DMC-7 | 125.7 | 757.3 | 0.4803 | 0.70784 | 11 | 0.70696 | 6.337 | 37.50 | 0.1022 | 0.51182 | 13 | −14.3 |
| XLZ-1 | 77.85 | 784.8 | 0.2871 | 0.70665 | 13 | 0.70612 | 3.472 | 20.88 | 0.1005 | 0.51194 | 13 | −12.1 |
| XLZ-2 | 83.86 | 776.0 | 0.3128 | 0.70665 | 13 | 0.70607 | 3.188 | 19.37 | 0.0995 | 0.51195 | 13 | −11.8 |
| XLZ-4 | 75.00 | 828.7 | 0.2619 | 0.70655 | 9 | 0.70607 | 2.954 | 18.55 | 0.0963 | 0.51197 | 14 | −11.4 |
| XLZ-6 | 75.30 | 808.8 | 0.2694 | 0.70654 | 10 | 0.70604 | 3.147 | 20.29 | 0.0938 | 0.51190 | 14 | −12.7 |
| FJZ-1 | 66.69 | 957.0 | 0.2017 | 0.70629 | 10 | 0.70592 | 4.881 | 28.79 | 0.1025 | 0.51179 | 15 | −15.0 |
| FJZ-2 | 73.97 | 847.7 | 0.2525 | 0.70615 | 11 | 0.70569 | 4.636 | 27.86 | 0.1006 | 0.51176 | 11 | −15.6 |
| FJZ-4 | 65.87 | 953.0 | 0.2000 | 0.70627 | 11 | 0.70590 | 4.433 | 26.46 | 0.1013 | 0.51176 | 11 | −15.7 |
| FJZ-6 | 66.34 | 958.2 | 0.2004 | 0.70628 | 10 | 0.70591 | 4.627 | 27.21 | 0.1028 | 0.51175 | 13 | −15.8 |
| QTJ-2 | 82.69 | 1097 | 0.2182 | 0.70716 | 11 | 0.70675 | 6.581 | 39.78 | 0.1000 | 0.51175 | 12 | −15.8 |
| QTJ-3 | 72.60 | 863.9 | 0.2431 | 0.70658 | 10 | 0.70675 | 4.195 | 24.09 | 0.1053 | 0.51171 | 13 | −16.7 |
| QTJ-4 | 62.68 | 861.8 | 0.2105 | 0.70666 | 14 | 0.70627 | 4.453 | 26.48 | 0.1017 | 0.51167 | 13 | −17.4 |
| QTJ-5 | 67.42 | 806.9 | 0.2418 | 0.70668 | 12 | 0.70623 | 5.200 | 30.20 | 0.1041 | 0.51169 | 15 | −17.0 |
| *LYRB* | | | | | | | | | | | | |
| YS-1 | 67.56 | 1346 | 0.1452 | 0.70669 | 11 | 0.70641 | 4.220 | 25.55 | 0.0999 | 0.51214 | 10 | −8.1 |
| YS-3 | 53.52 | 1414 | 0.1095 | 0.70670 | 13 | 0.70653 | 13.26 | 82.70 | 0.0970 | 0.51218 | 10 | −7.2 |
| TGS-2 | 50.17 | 1041 | 0.0326 | 0.70728 | 12 | 0.70720 | 9.729 | 52.95 | 0.1111 | 0.51201 | 11 | −10.8 |
| TGS-3 | 64.19 | 929.6 | 0.1998 | 0.70769 | 10 | 0.70734 | 8.738 | 47.69 | 0.1108 | 0.51198 | 10 | −11.3 |
| TGS-7 | 74.36 | 944.6 | 0.2277 | 0.70769 | 11 | 0.70723 | 10.17 | 53.34 | 0.1154 | 0.51198 | 12 | −11.4 |

Initial Sr and Nd isotopic ratios for STLF samples are calculated based on the zircon U–Pb ages obtained in this study, and for LYRB samples are calculated based on $t = 136$ Ma (Wang et al., 2004a).

Table 3
Pb isotopic data of adakites from the STLF and the LYRB reported in this study.

| Sample No. | $^{206}Pb/^{204}Pb$ | $2\sigma$ | $^{207}Pb/^{204}Pb$ | $2\sigma$ | $^{208}Pb/^{204}Pb$ | $2\sigma$ | $^{206}Pb/^{204}Pb(t)$ | $^{207}Pb/^{204}Pb(t)$ | $^{208}Pb/^{204}Pb(t)$ |
|---|---|---|---|---|---|---|---|---|---|
| *STLF* | | | | | | | | | |
| DMC-7 | 16.485 | 2 | 15.364 | 2 | 36.941 | 3 | 16.348 | 15.358 | 36.734 |
| XLZ-6 | 16.389 | 3 | 15.404 | 3 | 36.725 | 6 | 16.258 | 15.398 | 36.564 |
| FJZ-2 | 16.494 | 3 | 15.352 | 3 | 37.043 | 6 | 16.384 | 15.346 | 36.900 |
| FJZ-6 | 16.454 | 1 | 15.348 | 1 | 37.008 | 2 | 16.366 | 15.343 | 36.869 |
| *LYRB* | | | | | | | | | |
| YS-1 | 17.850 | 3 | 15.532 | 2 | 38.051 | 6 | 17.850 | 15.532 | 38.051 |
| YS-5 | 17.898 | 1 | 15.503 | 1 | 38.034 | 3 | 17.898 | 15.503 | 38.034 |
| TGS-2 | 17.828 | 4 | 15.545 | 4 | 38.058 | 8 | 17.828 | 15.545 | 38.058 |
| TGS-7 | 17.742 | 4 | 15.479 | 3 | 37.940 | 7 | 17.742 | 15.479 | 37.940 |

Initial Pb isotopic ratios of the STLF samples are calculated using the U, Th, and Pb contents determined by ICP-MS in this study and the zircon U–Pb ages obtained in this study (Table A1). The LYRB samples were determined for plagioclase common Pb.

petrogenesis of these two groups of adakites, and their implications for Cu–Au mineralization, are discussed below.

### 5.1. Geochemical differences and petrogenesis

#### *5.1.1. $K_2O$ contents and $K_2O/Na_2O$ ratios*

The major geochemical differences between the LYRB and STLF high-Mg adakites are summarized in Table 4. The LYRB adakites are sodic with $Na_2O = 3.2$ to 7.2 wt.% and $K_2O = 0.5$ to 4.1 wt.%. Their $K_2O/Na_2O$ ratios vary from 0.10 to 0.89 with an average of 0.6. The broad $K_2O/Na_2O$ range, coupled with high $Al_2O_3$ contents (average 16.1 wt.%), generally agree with oceanic slab-derived adakites (Fig. 6). These characteristics are also similar to those of experimental partial melts generated by melting of low-K MORB at pressures of 1–2 GPa and temperatures of $\leqslant$1100 °C (Rapp et al., 1991; Winther and Newton, 1991; Sen and Dunn, 1994; Wolf and Wyllie, 1994; Rapp and Watson, 1995; Prouteau et al., 2001). In contrast, the STLF adakites are mostly potassic with distinctly higher $K_2O$ contents (3.3–5.4 wt.%) and $K_2O/Na_2O$ (0.65–1.96; average 1.0) (Fig. 6). These features are similar to those of low-Mg adakitic rocks from the Dabie orogen (Fig. 6), which

Table 4
Summary of geochemical differences between the STLF and LYRB high-Mg adakites.

| | STLF | LYRB |
|---|---|---|
| Mineralization | ore-barren | ore-bearing |
| Age (Ma) | 132–125 | ~143–134 |
| $SiO_2$ (wt.%) | 56.2–69.5 | 56.3–69.9 |
| $Al_2O_3$ (wt.%) | avg. 14.9 | avg. 16.1 |
| $K_2O/Na_2O$ | 0.65–2.0 (avg. 1.0) | 0.1–0.89 (avg. 0.6) |
| MgO (wt.%) | 1.42–6.05 | 0.56–3.99 |
| Mg# | avg. 56 | avg. 45 |
| Cr (ppm) | 36.1–263 | 6.4–113 |
| Ni (ppm) | 15.5–121 | 3.7–64.6 |
| Sr (ppm) | 529–1040 | 490–2303 |
| Y (ppm) | 8–21 | 7–24 |
| Sr/Y | avg. 60 | avg. 85 |
| $(La/Yb)_N$ | avg. 28.2 | avg. 21.5 |
| Ce/Pb | avg. 3.8 | avg. 6.8 |
| Sr/La | avg. 19 | avg. 32 |
| $(^{87}Sr/^{86}Sr)_i$ | 0.7057–0.7077 | 0.7051–0.7099 |
| $\varepsilon_{Nd}(t)$ | −26.5 to −11.4 | −12.1 to −3.4 |
| $^{206}Pb/^{204}Pb(t)$ | 15.8–16.4 | 16.7–18.8 |

Age data are from this study (Table A1) and literature (Chen et al., 1991; Wang et al., 2006, 2007a; Huang et al., 2008; Zi et al., 2008; He et al., 2009; Li et al., 2009; Xie et al., 2009). Elemental and isotopic data are from this study (Tables 1–3) and literature (Tables A2–A5).

were derived from partial melting of eclogitic LCC rocks of the over-thickened mountain root (Wang et al., 2007b; He et al., 2010).

The differences in $K_2O$ contents and $K_2O/Na_2O$ between the LYRB and STLF adakites can be explained by the presence or absence of amphibole in sources. Because amphibole is the main K-bearing mineral, having much higher $K_2O$ than garnet and clinopyroxene in residual phases during high-pressure melting of metabasaltic rocks (e.g., Sen and Dunn, 1994; Rapp and Watson, 1995), the presence of amphibole in the residue can buffer the K concentration in the melt and thus, produce low-K silicic melts. For instance, oceanic adakites with Na-enrichment and K-depletion (low $K_2O/Na_2O$) are interpreted to be products of partial melting of the MORB compositions (e.g., amphibolites) with garnet + clinopyroxene + amphibole in the residual (Defant and Drummond, 1990; Rapp et al., 1991; Sen and Dunn, 1994; Rapp and Watson, 1995; Martin et al., 2005). In addition, some Na-rich adakitic rocks were also suggested to result from partial melting of newly underplated basaltic material with residues of garnet, clinopyroxene, and amphibole (Petford and Atherton, 1996). In contrast, given an eclogite residual assemblage without amphibole, partial melting of dry mafic LCC rocks (e.g., eclogites) would be expected to generate high K melts (Huang and He, 2010). Accordingly, the differences in $K_2O$ and $K_2O/Na_2O$ between the LYRB and STLF adakites may reflect the key role of water during melting, as only water-bearing melting has amphibole as a residual phase. The STLF adakites could originate from a dry eclogitic LCC, whereas the LYRB adakites likely originated from partial melting of hydrous oceanic crust with residual amphibole during melting.

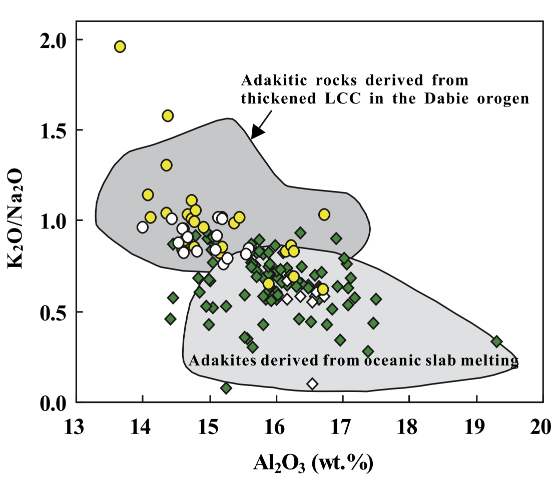


Fig. 6. $K_2O/Na_2O$ versus $Al_2O_3$ diagram comparing the LYRB adakites, the STLF adakites, thickened lower crust-derived low-Mg adakitic rocks from the Dabie orogen (Wang et al., 2007b; He et al., 2010), and oceanic slab-derived adakites (after Kamei et al., 2009). Data sources for STLF and LYRB samples are the same as in Fig. 3.

*5.1.2. MgO, Cr, Ni, and Mg#*

Both the LYRB and STLF adakites show relatively higher Mg# and MgO contents than the pristine experimental melts (Rapp et al., 1999) (Figs. 7 and 8). For example, almost all the LYRB adakites plot in the field of slab-derived adakites that are inferred to have interacted with the mantle wedge during ascent (e.g., Defant and Kepezhinskas, 2001) (Fig. 8). However, at a given $SiO_2$ the STLF adakites display higher Mg#, MgO, Cr, and Ni contents than the LYRB adakites and oceanic slab-derived adakites (Figs. 7 and 8). In particular, their Mg# (up to 67), Cr (up to 263 ppm) and Ni (up to 121 ppm) are equal to or even higher than those of late Mesozoic basaltic igneous rocks in the adjacent LYRB area (e.g., Mg# <58; Yan et al., 2008), and mafic dikes (e.g., Mg# <50) found in the adjacent Dabie orogen (Chen et al., 2002a; Wang et al, 2005; Huang et al., 2007; He et al., 2010). These observations, in conjunction with the absence of spatial-temporal association with mafic rocks, suggest that the high-Mg features of the STLF adakites were not derived from mixing with mafic magmas, but could be indicative of substantial interaction with the mantle.

There are broadly negative correlations between MgO and $SiO_2$ for both STLF and LYRB adakites (Fig. 8), which are nearly parallel to each other, although the former have systemically higher MgO contents than the latter at a certain $SiO_2$. This difference may reflect their difference in: (1) Mg# and MgO of initial magmas, (2) degrees of interaction with the mantle, (3) degrees of magma differentiation, and/or (4) extents of crustal contamination. Because these two groups of adakites were intruded into the Yangtze Block, more crustal contamination would produce higher contents of incompatible elements (e.g., potassium) (DePaolo, 1981), which is contradictory to what is observed (Fig. 6). Thus, the lower K contents of the LYRB adakites

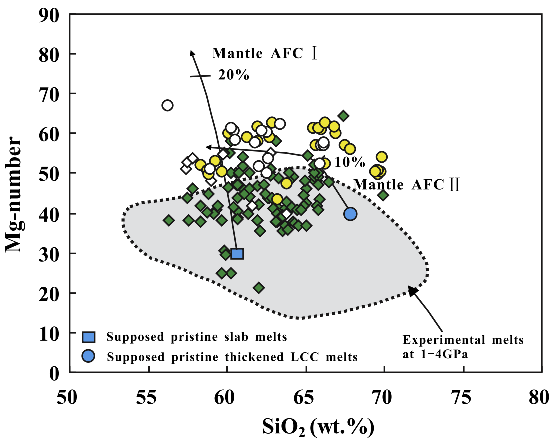


Fig. 7. Mg# versus $SiO_2$ diagram for adakites from the LYRB and STLF. The field for experimental melts at 1–4 GPa and Mantle AFC curves are after Rapp et al. (1999). The proportion of assimilated peridotite is also shown. Data sources are the same as in Fig. 3.

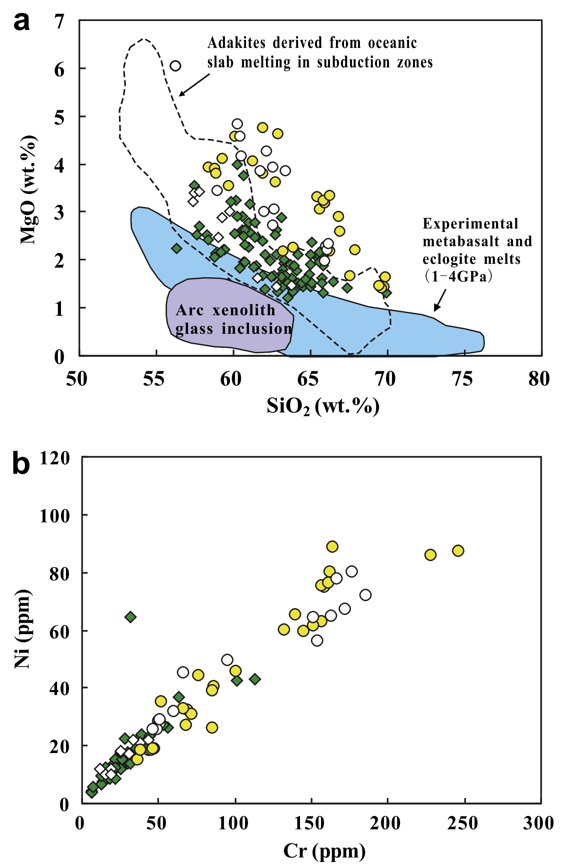


Fig. 8. (a) MgO versus $SiO_2$ diagram; (b) Cr versus Ni diagram. Both the STLF and LYRB adakites have MgO contents higher than those of the experimental melts, but the former display systemically higher Mg#, MgO, Cr and Ni contents at given $SiO_2$ than the latter and slab-derived adakites. Data sources for the STLF and LYRB adakites are the same as in Fig. 3. The field for adakites derived from slab melting is from Defant and Kepezhinskas (2001), for experimental melts is from Rapp et al. (1999), and for arc xenolith glass inclusion is from Schiano et al. (1995).

than the STLF adakites indicate that their lower Mg# and MgO were not derived from crustal contamination (Model (4)). Model (3) can also be excluded, because different degrees of magmatic differentiation of a similar initial magma cannot dramatically change MgO, Mg#, Cr, and Ni but leave $SiO_2$ unchanged (e.g., Ickert et al., 2009). Consequently, two remaining possibilities are that their initial magmas either have had different Mg# and MgO (Cr and Ni), or they experienced different degrees of interaction with the mantle during ascent.

Although experimental studies have shown that fluid-absent melting of basaltic rocks would generate melts with slightly higher MgO and Mg# than those of water-saturated melting (e.g., hydrous MORB) (Sen and Dunn, 1994; Rapp and Watson, 1995; Prouteau et al., 2001; Pertermann and Hirschmann, 2003; Xiong et al., 2006), the fact that the STLF adakites have MgO contents about twice as high as the LYRB adakites at a given $SiO_2$ (Fig. 8) appears not to be simply a result of source effect. Instead, different extents of interaction with the mantle, a process by which silicic melts can dramatically elevate their MgO and Mg# (e.g., Rapp et al., 1999; Prouteau et al., 2001), might play a crucial role in causing this difference. Although fully addressing this problem is beyond the scope of this study, here we propose a hypothesis. Since partial melts from hydrous MORB melting may have higher water contents than those from dry eclogite melting, the former (wet silicate melts) should have lower viscosity than the latter (dry silicate melts) (e.g., Lange, 1994). If true, the dry melts would be expected to migrate through the surrounding mantle more slowly than the wet melts, and thus presumably have a longer time and greater extent to interact with the mantle, resulting in their higher MgO (Cr and Ni) contents (Rapp et al., 1999). It is also possible that the wetter magmas were colder at their liquidus, and therefore less able to react with or assimilate peridotite. However, since the colder (wetter) magmas should quickly reach thermo-equilibrium with the surrounding mantle, the melt–rock interaction temperature would mainly depend on the temperature of lithospheric mantle. Therefore, we suggest that the fluxing ability of the two different magmas with respect to peridotite wall-rocks is more important. In any case, the observed differences of Mg#, MgO, Cr, and Ni between these two groups of adakites consistently reflect their difference in water amounts available in magma sources (i.e., the hydrous MORB for LYRB adakites and the dry eclogitic LCC for STLF adakites). This is also in good agreement with the conclusion based on their $K_2O$ and $K_2O/Na_2O$ differences as discussed above.

### *5.1.3. Trace elements*

The LYRB and STLF adakites share similar patterns of trace elements and rare earth elements, with enrichment in LREE relative to HREE, enrichment in LILE, depletion in HFSE (Nb, Ti, and Ta), and lacking or positive Eu anomalies (Fig. 4). These features are typical of adakitic rocks regardless of diverse origins. However, there are still prominent differences in several key trace elements between them (Table 4).

High Sr/Y and $(La/Yb)_N$ values are two most important parameters to identify adakites (Defant and Drummond, 1990; Martin et al., 2005; Moyen, 2009). The LYRB adakites are characterized by relatively low $(La/Yb)_N$ (average 21.5) but variable and high Sr/Y (29–201; average 85), which are comparable to oceanic adakites from subduction zones (Fig. 9). On the contrary, the STLF adakites exhibit higher $(La/Yb)_N$ (average 28.2 but up to 53) but lower Sr/Y (average 60) than the LYRB adakites and oceanic adakites (Fig. 9). Furthermore, they follow the trend defined by the thickened LCC-derived low-Mg adakitic rocks in the Dabie orogen (Wang et al., 2007b; He et al., 2010). This means that the ratio of Sr/Y to $(La/Yb)_N$ (i.e. the slope in Fig. 9) of the LYRB adakites and slab-derived adakites is approximately twice of that of the STLF and Dabie adakitic rocks. We note that these two different trends are mainly attributed to significantly higher Sr contents of the LYRB adakites than the STLF adakites (average 1112 versus 784 ppm; Table 4).

The positive correlation between Sr/Y and $(La/Yb)_N$ of the Dabie low-Mg adakitic rocks could be due to different degrees of partial melting of thickened LCC at high pressures, with absence of plagioclase in the residues (He et al., 2010). Theoretically, if Sr/Y and $(La/Yb)_N$ of an adakite magma are produced by various levels of partial melting of an eclogite or garnet amphibolite, they should define a positive correlation because under such conditions both Sr and La are incompatible whereas both Y and Yb are compatible in the garnet-bearing and plagioclase-free residues (e.g., Defant and Drummond, 1990; Rapp and Watson, 1995; Moyen, 2009). The consistent trend of the STLF adakites with the Dabie low-Mg adakitic rocks in the plot of Sr/Y versus $(La/Yb)_N$, thus, suggests that they both were derived from partial melting of the LCC of the Yangtze Block.

Despite some overlaps, many of the LYRB adakites display much higher Sr/Y than the STLF adakites at a given $(La/Yb)_N$ (Figs. 5 and 9), suggesting a decoupling of Sr/Y and $(La/Yb)_N$ in the LYRB adakites. Such a decoupling was unlikely to have been caused by plagioclase and garnet fractionation, because plagioclase fractionation would lower Sr/Y of the melts while garnet fractionation would increase not only Sr/Y but also $(La/Yb)_N$. Instead, this decoupling is most likely due to their parental magmas or magma sources having high Sr/Y but low $(La/Yb)_N$. Given that sediments on the ocean floor may have compositions equivalent to the upper continental crust (Plank and Langmuir, 1998), sediment involvement during oceanic crust melting would increase both these ratios and thus might not cause the decoupling. Consequently, the high Sr/Y but low $(La/Yb)_N$ suggests that the LYRB adakites originated from the subducted oceanic crust (MORB) experienced by low-temperature seawater alteration, which is a common process potentially elevating Sr of the altered MORB with little change in REE (e.g., Alt et al., 1986; Nakamura et al., 2007). For example, Kogiso et al. (1997) pointed out that N-MORB has ~90 ppm Sr while altered-MORB has significantly higher Sr contents of ~180 ppm. It should be noted, however, that the average LCC (Sr/Y ~22, La/Yb ~6; Rudnick and Gao, 2003) is remarkably more enriched in trace element compositions than the N-MORB (Sr/Y ~3, La/Yb ~0.8; Sun and McDonough,

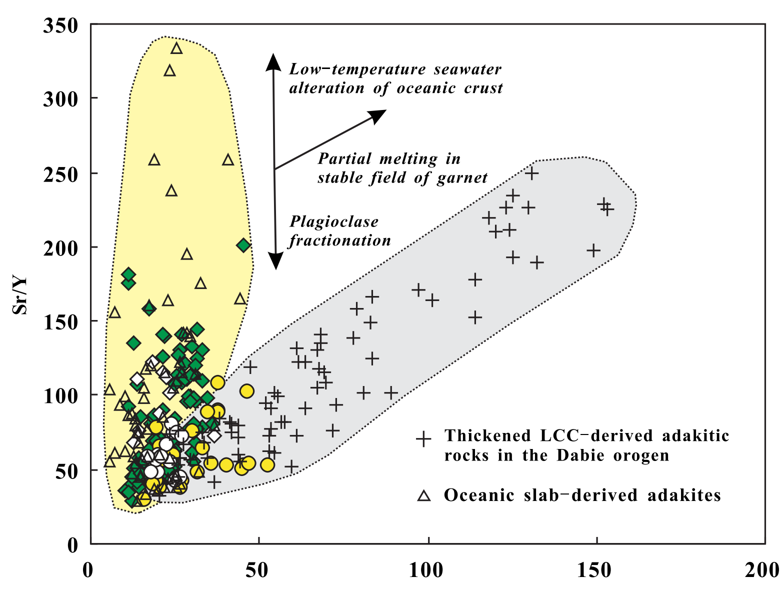


Fig. 9. Sr/Y versus $(La/Yb)_N$ diagram for adakites from the LYRB and STLF. Adakites related to slab melting in subduction zones (Puig et al., 1984; Defant and Drummond, 1990; Defant et al., 1991; Morris, 1995; Stern and Kilian, 1996; Aguillón-Robles et al., 2001; Beate et al., 2001) and thickened lower crust-derived low-Mg adakitic rocks in the Dabie orogen (Wang et al., 2007b; He et al., 2010) are also shown for comparison. The positive correlation between Sr/Y and $(La/Yb)_N$ in the Dabie adakitic rocks was interpreted to reflect partial melting of the eclogitic lower crust at various degrees (He et al., 2010).

1989). Therefore, the low $(La/Yb)_N$ but variable high Sr/Y of the LYRB adakites and slab-derived adakites, relative to adakites from the STLF and the Dabie orogen (Fig. 9), can be mainly due to (1) much lower Sr/Y and La/Yb of the N-MORB than the LCC, and (2) Sr elevation of the subducted oceanic slabs by interaction with seawater at low-temperatures. Sen and Dunn (1994) found that Sr/Y of natural adakites are about twice of those of adakitic melts in melting models with an N-MORB starting composition, and suggested that oceanic adakites are derived from melting of a source with higher Sr/Y than N-MORB. Our explanation of the Sr/Y and La/Yb decoupling in the LYRB adakites and some oceanic adakites as a result of oceanic crust alteration is also consistent with the observation in Cenozoic adakites from Vizcaino Penisula in Mexico, which have relatively low $(La/Yb)_N$ (10.4–23.0) but variable high Sr/Y ratios (62–164). These rocks were proposed to result from partial melting of low-temperature seawater-altered oceanic crust, based upon their high radiogenic Pb and Sr isotope compositions (Aguillón-Robles et al., 2001).

Furthermore, we use a Ce/Pb–Sr/La diagram (Fig. 10) to distinguish rocks derived from subducted oceanic crust and those derived from LCC. This is based on the observations that continental crust has lower Ce/Pb (~4–5; Taylor and McLennan, 1985; Rudnick and Gao, 2003) than oceanic crust (~24; Sun and McDonough, 1989), and altered oceanic crust has much higher Sr/La than LCC, due to LREE depletion of N-MORB and Sr enrichment by seawater alteration. The average Sr/La of the LYRB adakites is higher than that of the STLF adakites (32 versus 19). As illustrated in Fig. 10, the LYRB adakites exhibit a wide range of Ce/Pb ratios with an average of 6.8 also clearly higher than that of the STLF adakites (3.8). The latter is almost the same as that of the thickened LCC-derived adakitic rocks in the Dabie orogen (3.8; Wang et al., 2007b; He et al., 2010), consistent with a similar source in the LCC of the Yangtze Block. This value is also generally consistent with that of the average LCC. However, because crustal

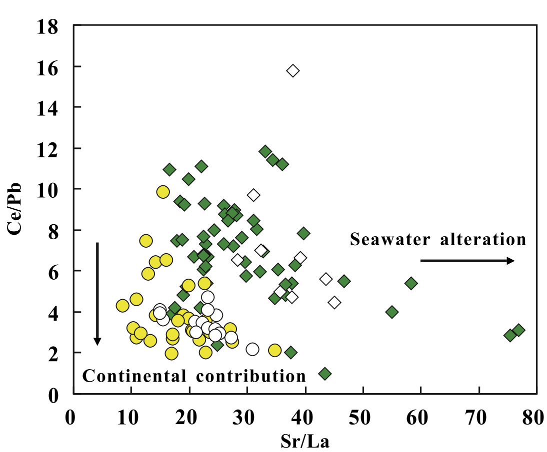


Fig. 10. Sr/La versus Ce/Pb diagram for the LYRB and STLF adakites. The LYRB adakites have Sr/La and Ce/Pb ratios higher than the STLF adakites, reflecting their different sources from altered oceanic crust and ancient lower continental crust, respectively. Data sources are same as in Fig. 3.

contamination (if any) may lower Ce/Pb ratios of the magmas, the variable and high Ce/Pb of the LYRB adakites do not support a LCC origin. Instead, this signature suggests an origin from subducted oceanic crust with addition of sediments during melting. This conclusion is also supported by low Nb/U (average 5.3) and high Ba/Th ratios (average 136) of the LYRB adakites, which probably indicate contribution from sediments (e.g., Plank and Langmuir, 1998).

*5.1.4. Sr, Nd, and Pb isotopic compositions*

Initial Sr–Nd isotopic compositions of the LYRB adakites differ from those of the STLF adakites and the Yangtze LCC-derived low-Mg adakitic rocks (Wang et al., 2004a, 2007b; Guo et al., 2006; He et al., 2010) (Fig. 11). Given that the melt/mantle interaction that mainly consumes olivines in the mantle (Rapp et al., 1999) may not significantly change Sr–Nd isotopic ratios of resulting magmas (e.g., Huang et al., 2008; Yang and Li, 2008), different Sr–Nd isotopic compositions of these two groups of adakites must reflect their different source features. Typically trending towards the EM-1 end member, and similar to the Yangtze LCC-derived adakitic rocks (Fig. 11), the STLF adakites could be derived from partial melting of the Yangtze LCC. In contrast, isotopic signatures of the LYRB adakites are typically displaced toward the EM-2 end member, reflecting the important role of sediments in magma source. The LYRB adakites have heavy oxygen isotopic compositions ($\delta^{18}O = +8.7$ to $+10.9$; Chen et al., 1993), which further supports sediment involvement in the magma source. In addition, these isotopic signatures are similar to those of the early Cretaceous mafic rocks formed by melting of the lithospheric mantle beneath the LYRB, which was previously metasomatized by subducted slab-derived melts/fluids (Fig. 11). Therefore, the isotopic signature of the LYRB adakites may mainly reflect that of subducted slab.

Lead isotopic data provide additional insights into the different sources of these two groups of adakites. The low radiogenic Pb of the STLF adakites (Fig. 12) are the typical features of the ancient LCC, consistent with their derivation from partial melting of the Yangtze LCC. In contrast, the LYRB adakites show much higher radiogenic Pb (Fig. 12). These Pb isotopic signatures mostly overlap with MORB (Hofmann, 2003), consistently showing that the LYRB adakites originated from oceanic crust rather than ancient LCC. Some samples have Pb isotopic compositions similar to marine sediments (Fig. 12), suggesting a mixture of sediments and basaltic oceanic crust, consistent with the conclusions based on Sr and Nd as well as O isotopes.

In conclusion, the differences in elemental and isotopic compositions between the STLF and LYRB adakites suggest distinct petrogenesis. The STLF adakites were likely derived from partial melting of the delaminated dry mafic LCC of the Yangtze Block, followed by interaction with the mantle peridotites during ascent (Huang et al., 2008; Zi et al., 2008; He et al., 2009; this study). The distinct geochemical characteristics of the LYRB adakites are best interpreted to be produced by partial melting of the subducted oceanic slab plus sediments, and subsequent interaction with the mantle during ascent. Our study does not support the interpretation that the LYRB adakites were

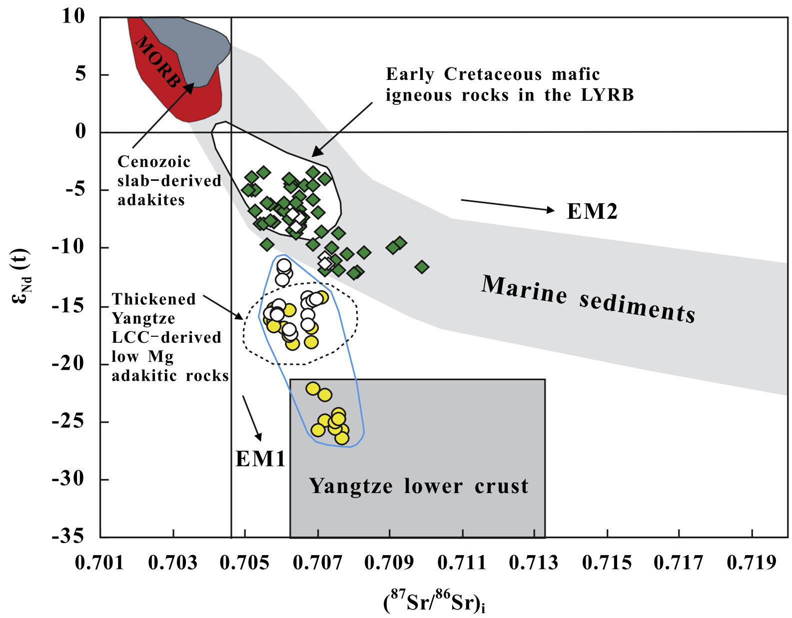


Fig. 11. Initial Sr–Nd isotopic compositions of adakites from the LYRB and STLF. Cenozoic slab-derived adakites (Defant and Kepezhinskas, 2001), thickened Yangtze lower crust-derived low-Mg adakitic rocks, e.g., in the Dabie orogen (Wang et al., 2007b; He et al., 2010), in the Sulu belt (Chuzhou; Guo et al., 2006) and in the LYRB (Hongzhen; Wang et al., 2004a), and early Cretaceous mafic igneous rocks in the LYRB (Yan et al., 2008) are shown for comparison. Data sources: LYRB and STLF adakites, this study (Table 2) and the literature (Supplementary Table A4); MORB and marine sediments, Hofmann (2003); Yangtze lower crust, Jahn et al. (1999).

from the delaminated Yangtze LCC as previously proposed (e.g., Xu et al., 2002; Wang et al., 2003, 2004a, 2004b, 2006, 2007a).

### 5.2. The relationship between early Cretaceous adakites and basaltic igneous rocks in the LYRB

Several studies proposed that some of the LYRB adakites might be formed by fractional crystallization of basaltic magmas, with or without crustal contamination (Wang et al., 2004; Xie et al., 2008; Li et al., 2009). The major evidence supporting the fractional crystallization model is the similarity of Sr–Nd–Pb isotopic compositions between adakites and basaltic igneous rocks in the LYRB (Figs. 11 and 12). However, the lack of temporal association between the early Cretaceous adakites and basaltic igneous rocks in the LYRB does not support a direct petrogenetic connection between them. The intermediate-felsic adakitic intrusions in the LYRB were formed generally before 134 Ma and are rarely associated with basaltic igneous rocks (Chen et al., 1993; Wang et al., 2004a; Yan et al., 2008, 2009). Recent high-precision U–Pb zircon dating further confirms that basaltic igneous rocks consisting of gabbros and alkali volcanic rocks throughout the LYRB were formed at 131–125 Ma with a peak of ~130 Ma (Zhang et al., 2003; Xie et al., 2006; Yan et al., 2009), which are clearly younger than the adakites in the LYRB (~143–134 Ma).

Early studies have suggested that the early Cretaceous mantle domain beneath the LYRB, as sampled by high-K basaltic igneous rocks, shows a clear EM2-like Sr–Nd–Pb isotope signature (e.g., Yan et al., 2008, 2009; Wang et al., 2006). This implies previous metasomatism of the mantle by slab melts/fluids. Nevertheless, the timing and process of this metasomatism event has not been explicitly constrained. The similarity in Sr–Nd–Pb isotopes between adakites and basaltic igneous rocks in the LYRB may provide important insights into these issues. Our results suggest that metasomatism of the underlying mantle beneath the LYRB could be related to melts/fluids derived from the subducted oceanic slab at the early Cretaceous. The metasomatized mantle was subsequently melted with generation of the younger basaltic lavas or their intrusive equivalents. This accounts well for the similar Sr–Nd–Pb isotopic signatures of basaltic igneous rocks with the recycled crustal rocks (e.g., in the Mediterranean area, Lustrino, 2005; in the North China Craton, Huang et al., 2007).

### 5.3. Tectonic implications from the two groups of high-Mg adakites in eastern China

Although density of eclogitic LCC could be greater than the underlying asthenospheric mantle, it is unlikely that the density contrast is large enough for foundering of the whole rigid lithosphere (Huang et al., 2008). The characteristic distribution of the STLF high-Mg adakites (Fig. 1) implies the possible role of movement of the Tan-Lu fault in triggering delamination of the dense eclogitic LCC. Strike-slip movement of the Tan-Lu fault in the late Jurassic to early Cretaceous (Zhu et al., 2005; Wang, 2006) may be the principal cause of foundering of the eclogitic lower crustal fragments along this fault (Huang et al., 2008). Notably, the STLF adakitic intrusions become slightly younger with the distance to the Tan-Lu fault (Fig. 1). This geographic

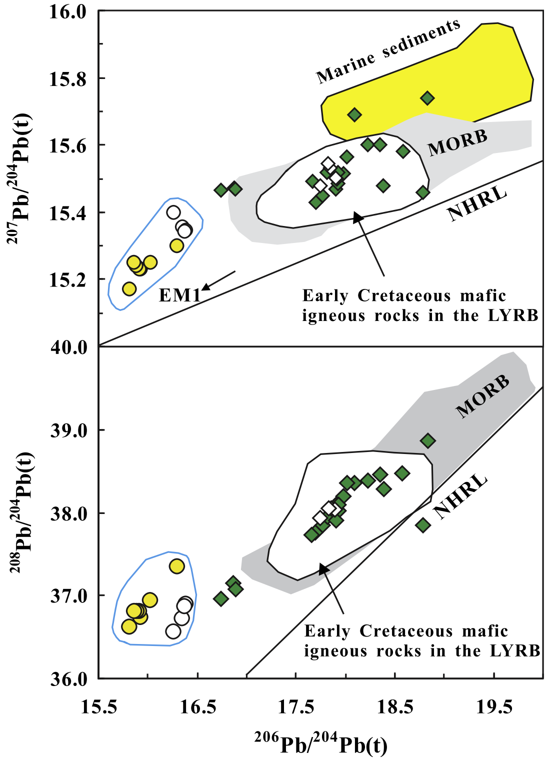


Fig. 12. Initial Pb isotopic compositions of adakites from the LYRB and the STLF. Data are from this study (Table 3) and literature (Supplementary Table A5; Chen et al., 1993; Xu et al., 2002; Wang et al., 2006; Huang et al., 2008; Zhao et al., 2010). Early Cretaceous mafic igneous rocks in the LYRB (Yan et al., 2008) are also shown for comparison. The Northern Hemisphere Reference line (NHRL) is after Zindler and Hart (1986). Data sources for MORB and marine sediments are the same as in Fig. 11.

distribution and age variation among the STLF adakites also support that the foundering of the eclogitic LCC was initiated from the region close to the Tan-Lu fault.

The late Mesozoic intensive magmatism in the LYRB is usually attributed to an extensional tectonic setting (e.g., Wang et al., 2004a; Wang et al., 2006, 2007a; Yan et al., 2008, 2009; Xie et al., 2008; Li et al., 2009), as suggested by the occurrence of early Cretaceous high-K volcanic rocks and the development of expanding basins. Recent studies, however, suggested that eastern China had become an active continental margin from the Jurassic to the Cretaceous, which was closely associated with subduction of the Pacific plate (Li and Li, 2007; Sun et al., 2007). Li and Li (2007) proposed a model of Mesozoic flat-slab subduction of the Pacific plate to explain the broad intercontinental orogen in the South China Block and referred that the early Cretaceous adakites in the LYRB might be formed by slab melting. More recently, Ling et al. (2009) proposed a model of mid-ocean ridge (MOR) subduction in central-eastern China at the early Cretaceous, based on different drifting directions and rates of the Izanagi plate (Maruyama et al., 1997) and the Pacific plate (Sun et al., 2007). The MOR between these two plates was estimated to be drifting towards eastern China in a west or southwest direction, which had passed through or very close to the LYRB at about 140 Ma. Additionally, Ling et al. (2009) noted that the early Cretaceous adakites, basaltic igneous rocks including Nb-enriched basalts (NEBs), and A-type granites in the LYRB are characteristically distributed into several separate belts, but all are developed in a nearly east-west direction. These characteristic distributions had been suggested to support the MOR model and interpret the wide occurrence of high-K volcanic rocks and expanding basins. Our current study of the LYRB adakites presents direct geochemical evidence for oceanic plate subduction and slab melting in the LYRB at the early Cretaceous, which provides a new constraint on the MOR model, or any further reconstruction of the plate subduction in the LYRB.

### 5.4. Implications for Cu–Au mineralization

Chalcophile elements (e.g., Cu and Au) are highly compatible in magmatic sulfide phases, in contrast to their general incompatible behavior in silicate and oxide minerals (Fleet et al., 1996; Ballard et al., 2002). For this reason, removal of them from the mantle can only occur when the sulfide dominant in melt compositions is transformed to the sulfate-dominant under oxidized conditions (Ballard et al., 2002; Mungall, 2002). It has been widely accepted that slab-derived melts/fluids have high oxygen fugacities and thus potentially favor Cu–Au mineralization (Oyarzun et al., 2001; Ballard et al., 2002; Mungall, 2002; Kelley and Cottrell, 2009). This is supported by empirical association between porphyry Cu–Au ore deposits and adakitic intrusions in subduction zones around the world (Thiéblemont et al., 1997; Sajona and Maury, 1998; Oyarzun et al., 2001; Imai, 2002; Gonzalez-Partida et al., 2003; Rae et al., 2004). Mungall (2002) also suggested that if an arc magma has log $fo_2$ > SSO (sulfide-sulfur oxide buffer), it must contain a component of melted oceanic crust, i.e., adakitic melts or supercritical fluids.

The genetic links between adakites and their associated porphyry Cu–Au deposits in the LYRB remain a subject of considerable debate. This is mainly due to the large discrepancy between petrogenetic interpretations of the host adakites. Recently, several studies (Wang et al., 2003, 2004a, 2004b, 2007a) performed systematic geochemical comparisons between the ore-barren low-Mg adakitic granitoids in central-eastern China (e.g., in the Dabie orogen; Fig. 1) and the LYRB adakites to explain the genesis of Cu–Au deposits in the LYRB. These authors concluded that the low-Mg granitoids derived directly from LCC melting had not passed through the fertile mantle, so that they are not able to generate Cu–Au mineralization. In contrast, the LYRB adakites, which might have ascended through the fertile mantle via LCC delamination as proposed by these authors, could have transferred Cu and Au from the mantle to the crust. Such an explanation is mainly based on a hypothesis that the LCC-derived magmas may also carry the oxidizing potential, e.g., having elevated $Fe_2O_3$ content (Wang et al., 2006, 2007a). This conclusion, however, is challenged by the observation of the ore-barren high-Mg adakites from the STLF.

As discussed in this study, the STLF high-Mg adakites most likely originated from partial melting of the Yangtze

LCC via delamination, but none of them show any relationship with Cu–Au ore deposits (Huang et al., 2008; Zi et al., 2008; He et al., 2009; this study). This suggests that although the LCC-derived magmas may have interacted with the mantle, they did not give rise to Cu–Au mineralization. It is not surprising because the thickened mafic LCC should be relatively dry due to its general lithology of granulite- or eclogite-facies rocks, which generally contain little $H_2O$ (e.g., Xia et al., 2006; Yang et al., 2008), particularly in the case favoring delamination. This is consistent with distinctly high $K_2O/Na_2O$ and MgO (Cr, Ni) in the STLF high-Mg adakites suggesting dry eclogite sources. We therefore conclude that adakitic melts derived from partial melting of the delaminated or recycled LCC are not favorable for Cu–Au mineralization.

In sharp contrast, the LYRB adakites could be genetically associated with partial melting of subducted altered oceanic crust. Thus, the partial melts potentially have high oxygen fugacity ($fo_2$) (Jugo et al., 1999; Mungall, 2002; Kelley and Cottrell, 2009). Studies of trace elemental compositions of zircons from the LYRB adakites show high positive Ce anomalies (Xie et al., 2009), also suggesting magma formation at an oxidized environment. Consequently, the high $fo_2$ would facilitate destabilization of mantle sulfides to release their Cu–Au that are mainly hosted in sulfides, and contribute to subsequent enrichment of Cu–Au in the magmas. The large-scale Cu–Au ore deposits in the LYRB could thus be due to oceanic slab subduction and melting. The new understanding of the genetic links between adakites and relevant Cu–Au deposits in the LYRB in central-eastern China is also consistent with many studies of ore-bearing adakites in modern subduction zones around the world (Thiéblemont et al., 1997; Sajona and Maury, 1998; Oyarzun et al., 2001; Imai, 2002; Gonzalez-Partida et al., 2003; Rae et al., 2004). This provides an important exploration guide for Cu–Au deposits, especially in the LYRB.

## 6. CONCLUSIONS

A comprehensive geochemical comparison between early Cretaceous ore-bearing high-Mg adakites from the LYRB and ore-barren high-Mg adakites from the adjacent STLF in central-eastern China reveals different petrogenesis, which provides important insights into the genetic relationships between adakites and Cu–Au mineralization.

(1) The STLF adakites have the ancient LCC-like Sr–Nd–Pb isotopic signature and exhibit a good positive correlation between high Sr/Y and $(La/Yb)_N$. The high $K_2O$, Mg#, MgO, Cr and Ni and low Ce/Pb and Sr/La ratios indicate that their initial magmas were derived from partial melting of delaminated eclogitic LCC under dry condition, followed by interaction with the mantle.
(2) The LYRB adakites have an EM2-like Sr–Nd–Pb isotopic signature and relatively low $(La/Yb)_N$ but variable high Sr/Y, Sr/La and Ce/Pb ratios, distinct from magmas from either the thickened or delaminated LCC but similar to oceanic adakites from slab melting. In addition, their lower $K_2O/Na_2O$, Mg# and MgO, Cr, and Ni contents at given $SiO_2$ compared to the STLF adakites are also similar to oceanic adakites. The LYRB adakites were derived from partial melting of hydrous altered oceanic crust with sediments, not supporting a derivation by partial melting of the delaminated LCC proposed in previous studies.
(3) The early Cretaceous high-Mg adakites in central-eastern China may be related to subduction of the Pacific plate. Melting of the subducted oceanic crust produced adakitic magmatism in the LYRB. Northwestern subduction of the Izanagi plate in early Cretaceous induced the development of Tan-Lu fault and triggered the foundering of the lower crustal fragments near the fault zone. The delaminated LCC was later partially melted to generate the STLF high-Mg adakites.
(4) The Cu–Au mineralization in the LYRB was likely related to oceanic subduction and slab melting. While the ancient LCC-derived magma, regardless of having interacted with the mantle or not, does not favor Cu–Au mineralization.

## ACKNOWLEDGMENTS

We are grateful to Xiaoyong Yang, Yilin Xiao, Shichao An for their help with field investigations. We thank Zhenhui Hou, A. Reitz, G. Hartmann, Chaofeng Li, Jinrong Li, Shizhen Li, Xianhua Li, Qiuli Li and Yu Liu for assistance with element analysis, Sr, Nd and Pb isotope measurement and zircon U-Pb dating, and Jingao Liu for discussion. We thank three anonymous reviewers for constructive comments and Rich Walker for efficient editing that have helped improve the manuscript. We specially thank the anonymous reviewer for polishing English. S.-A. Liu thanks Fang-Zhen Teng for helpful discussion on an early draft of this paper. This work was supported by Academy of Science of China (No. KZCX1-YW-15-3), the State Key Basic Research Development Program (No. 2009CB825002) and National Nature Science Foundation of China (No. 90814008 and 40773013).

## APPENDIX A. SUPPLEMENTARY DATA

Supplementary data associated with this article can be found, in the online version, at doi:10.1016/j.gca.2010.09.003.

## REFERENCES

Aguillón-Robles A., Caimus T., Bellon H., Maury R. C., Cotton J., Bourgois J. and Michaud F. (2001) Late miocene adakites and Nb-enriched basalts from Vizcaino Peninsula, Mexico: indicators of East Pacific Rise subduction below southern Baja California. *Geology* **29**, 531–534.

Alt J. C., Honnorez J., Laverne C. and Emmermann R. (1986) Alteration of a 1 km section through the upper oceanic crust, DSDP Hole 504B: the mineralogy, chemistry, and evolution of basalt-seawater interactions. *J. Geophys. Res.* **91**, 10309–10335.

Ballard J. R., Palin J. M. and Campbell I. H. (2002) Relative oxidation states of magmas inferred from Ce(IV)/Ce(III) in zircon: application to porphyry copper deposits of northern Chile. *Contrib. Mineral. Petrol.* **144**, 347–364.

Beate B., Monzier M., Spikings R., Cotton J., Silva J., Bourdon E. and Eissen J. (2001) Mio–Pliocene adakite generation related to flat subduction in southern Ecuador: the Quimsacocha volcanic center. *Earth Planet. Sci. Lett.* **192**, 561–570.

Black L. P., Kamo S. L., Allen C. M., Davis D. W., Aleinikoff J. N., Valley J. W., Mundil R., Campbel I. H., Korsch R. J., Williams I. S. and Foudoulis Chri (2004) Improved $^{206}Pb/^{238}U$ microprobe geochronology by the monitoring of a trace-element-related matrix effect; SHRIMP, ID-TIMS, ELA-ICP-MS and oxygen isotope documentation for a series of zircon standards. *Chem. Geol.* **205**, 115–140.

Borisova A. Yu., Pichavant M., Polvé M., Wiedenbeck M., Freydier R. and Candaudap F. (2006) Trace element geochemistry of the 1991 Mt. Pinatubo silicic melts, Philippines: implications for ore-forming potential of adakitic magmatism. *Geochim. Cosmochim. Acta* **70**, 3702–3716.

Chen B., Jahn B. M. and Wei C. J. (2002a) Petrogenesis of mesozoic granitoids in the Dabie UHP complex, central china: trace element and Nd–Sr isotope evidence. *Lithos* **60**, 67–88.

Chen F., Siebel W., Satir M., Terzioglu N. and Saka K. (2002b) Geochronology of the Karadere basement (NW Turkey) and implications for the geological evolution of the Istanbul zone. *Int. J. Earth Sci.* **91**, 469–481.

Chen J. F., Li X. M., Zhou T. X. and Foland K. A. (1991) $^{40}Ar/^{39}Ar$ dating of the Yueshan diorite, Anhui province, and the estimated formation time of the associated ore deposit. *Geoscience* **5**, 91–99 (in Chinese with English abstract).

Chen, J. F., Zhou, T. X., Zhang, X., Xing, F. M., Xu, X., Li, X. M. and Xu, L. H. (1993) Isotopic geochemistry of copper-bearing rocks from middle–lower area of Yangtze. *The Study of Isotopic Geochemistry*. Zhejiang University Press, Hangzhou. pp. 214–229 (in Chinese).

Chiaradia M., Merino D. and Spikings R. (2009) Rapid transition to long-lived deep crustal magmatic maturation and the formation of giant porphyry-related mineralization (Yanacocha, Peru). *Earth Planet. Sci. Lett.* **258**, 593–604.

Defant M. J. and Drummond M. S. (1990) Derivation of some modern arc magmas by melting of young subducted lithosphere. *Nature* **347**, 662–665.

Defant M. J., Richerson P. M., DeBoer J. Z., Stewart R. H., Maury R. C., Bellon H., Drummond M. S., Feigenson M. D. and Jackson T. E. (1991) Dacite genesis via both slab melting and differentiation: petrogenesis of La Yegueda volcanic complex. *Panama. J. Petrol.* **32**, 1101–1142.

Defant M. J. and Kepezhinskas P. (2001) Evidence suggests slab melting in arc magmas. *EOS (Transactions, American Geophysical Union)* **82**, 65–69.

DePaolo D. J. (1981) Trace elements and isotopic effects of combined wallrock assimilation and fractional crystallization. *Earth Planet. Sci. Lett.* **53**, 189–202.

Fleet M. E., Crocket J. H. and Stone W. E. (1996) Partitioning of platinumgroup elements (Os, Ir, Ru, Pt, Pd) and gold between sulfide liquid and basalt melt. *Geochim. Cosmochim. Acta* **60**, 2397–2412.

Gonzalez-Partida E., Levresse G., Carrillo-Chavez A., Cheilletz A., Gasquet D. and Jones D. (2003) Paleocene adakite Au-Fe bearing rocks, Mezcala, Mexico: evidence from geochemical characteristics. *J. Geochem. Explor.* **80**, 25–40.

Guo F., Fan W. M. and Li C. W. (2006) Geochemistry of late Mesozoic adakites from the Sulu belt, eastern China: magma genesis and implications for crustal recycling beneath continental collisional orogens. *Geol. Mag.* **143**, 1–13.

He X. X., Zhu X. K., Yang C. and Tang S. H. (2005) High-precision analysis of Pb isotope ratios using MC–ICP–MS. *Acta. Geoscientica. Sinica* **26**, 19–22.

He, Y. S., Li, S. G., Hefos, J. and Schoenberg, I. (2009) Nd isotopic compositions of adakites from Dabieshan: Implications for the subducted mafic lower crust of the South China Block. *Geochim. Cosmochim. Acta* A507.

He, Y. S., Li, S. G., Hoefs, J., Huang, F. and Liu, S.-A. (2010) Partial melts from thick lower continental crust: geochemical characterization and identification. *Geochim. Cosmochim. Acta* A392.

Hofmann A. W. (2003) Sampling mantle heterogeneity through oceanic basalts: isotopes and trace elements. In *The Mantle and Core. Treatise on Geochemistry* (ed. R. W. Carlson). Elservier-Pergamon, Oxford, pp. 61–101.

Hou Z. H. and Wang C. X. (2007) Determination of 35 trace elements in geological samples by inductively coupled plasma mass spectrometry. *J. Uiv. Sci. Tech. China* **37**, 940–944.

Hou Z. Q., Pan X. F., Yang Z. M. and Qu X. M. (2007) Porphyry Cu–(Mo–Au) deposits not related to oceanic-slab subduction: examples from Chinese porphyry deposits in continental settings. *Geoscience* **21**, 332–351 (in Chinese with English abstract).

Huang F., Li S. and Yang W. (2007) Contributions of the lower crust to Mesozoic mantle-derived mafic rocks from the North China Craton: implications for lithospheric thinning. *J. Geol. Soc. London* **280**, 55–75.

Huang F., Li S., Dong F., He Y. and Chen F. (2008) High-Mg adakitic rocks in the Dabie orogen, central China: implications for foundering mechanism of lower continental crust. *Chem. Geol.* **255**, 1–13.

Huang F. and He Y. S. (2010) Partial melting of dry mafic lower continental crust: constraints on formation of C-type adakites. *Chin Sci Bull* **55**, 2428–2439.

Imai A. (2002) Metallogenesis of porphyry Cu deposits of the western Luzon arc, Philippines: K-Ar ages, $SO_3$ contents of microphenocrystic apatite and significance of intrusive rocks. *Resource Geol.* **52**, 147–161.

Ickert R. B., Thorkelson D. J., Marshall D. D. and Ullrich T. D. (2009) Eocene adakitic volcanism in southern British Columbia: remelting of arc basalt above a slab window. *Tectonophysics* **464**, 164–185.

Irvine T. N. and Baragar W. R. (1971) A guide to the chemical classification of the common volcanic rocks. *Can. J. Earth Sci.* **8**, 523–548.

Jugo P. J., Candela P. A. and Piccoli P. M. (1999) Magmatic sulfides and Au:Cu ratios in porphyry deposits: an experimental study of copper and gold partitioning at 850 °C, 100 MPa in a haplogranitic melt-pyrrhotite-intermediate solid solution-gold metal assemblage, at gas saturation. *Lithos* **46**, 573–589.

Jahn B. M., Wu F. Y., Lo C. H. and Tsai C. H. (1999) Crust-mantle interaction induced by deep subduction of the continental crust: geochemical and Sr–Nd isotopic evidence from post-collisional mafic-ultramafic intrusions of the northern Dabie complex, central China. *Chem. Geol.* **157**, 119–146.

Kamei A., Miyake Y., Owada M. and Kimura J.-I. (2009) A pseudo adakite derived from partial melting of tonalitic to granodioritic crust, Kyushu, southwest Japan arc. *Lithos* **112**, 615–625.

Kelley K. A. and Cottrell E. (2009) Water and the oxidation state of subduction zone magmas. *Science* **325**, 605–607.

Kogiso T., Tatsumi Y. and Nakano S. (1997) Trace element transport during dehydration processes in the subducted oceanic crust: 1. Experiments and implications for the origin of ocean island basalts. *Earth Planet. Sci. Lett.* **148**, 193–205.

Lange R. A. (1994) The effect of $H_2O$, $CO_2$, and F on the density and viscosity of silicate melts. *Rev. Mineral.* **30**, 331–360.

Li J. W., Zhao X. F., Zhou M. F., Ma C. Q., Sergio de Souza Z. and Vasconcelos P. (2009) Late Mesozoic magmatism from Daye region, eastern China: U-Pb ages, petrogenesis, and geodynamic implications. *Contrib. Mineral. Petrol.* **157**, 383–409.

Li Q.-L., Li X.-H., Liu Y., Wu F.-Y., Yang J.-H. and Mitchell R. H. (2010) Precise U–Pb and Th–Pb age determination of kimberlitic perovskites by secondary ion mass spectrometry. *Chem. Geol.* **269**, 396–405.

Li S. G., Xiao Y., Liu D., Chen Y., Ge N., Zhang Z., Sun S., Cong B., Zhang R., Hart S. R. and Wang S. (1993) Collision of the North China and Yangtze Blocks and formation of coesite-bearing eclogites: timing and processes. *Chem. Geol.* **109**, 89–111.

Li S. G., Jagoutz E., Chen Y. Z. and Li Q. L. (2000) Sm–Nd and Rb–Sr isotopic chronology and cooling history of ultrahigh pressure metamorphic rocks and their country rocks at Shuanghe in the Dabie Mountains, Central China. *Geochim. Cosmochim. Acta* **64**, 1077–1093.

Li Z. X. and Li X. H. (2007) Formation of the 1300-km-wide intracontinental orogen and postorogenic magmatic province in Mesozoic South China: A flat-slab subduction model. *Geology* **35**, 179–182.

Ling M. X., Wang F. Y. and Ding X., et al. (2009) Cretaceous ridge subduction along the Lower Yangtze River Belt, eastern China. *Econ. Geol.* **104**, 303–321.

Liu S.-A., Teng F.-Z., He Y., Ke S. and Li S. (2010) Investigation of magnesium isotope fractionation during granite differentiation: Implication for Mg isotopic composition of the continental crust. *Earth Planet. Sci. Lett.* **297**, 646–654.

Ludwig, K. R. (2001) Users Manual for Isoplot/Ex (rev.2.4.9): A geochronological Toolkit for Microsoft Excel. Berkeley Geochronology Center. Special Publication, No. 1a: 55 pp.

Lustrino M. (2005) How the delamination and detachment of lower crust can influence basaltic magmatism. *Earth Sci. Rev.* **72**, 21–38.

Mao J. W., Wang Y. T., Lehmann B., Yu J. J., Du A. D., Mei Y. X., Li Y. F., Zang W. S., Stein H. J. and Zhou T. F. (2006) Molybdenite Re–Os and albite $^{40}Ar/^{39}Ar$ dating of Cu–Au–Mo and magnetite porphyry systems in the Yangtze River valley and metallogenic implications. *Ore Geol. Rev.* **29**, 307–324.

Martin H., Smithies R. H., Rapp R., Moyen J. F. and Champion D. (2005) An overview of adakite, tonalite-trondhjemiten–granodiorite (TTG), and sanukitoid: relationships and some implications for crustal evolution. *Lithos* **79**, 1–24.

Maruyama S., Isozaki Y., Kimura G. and Terabayashi M. (1997) Paleogeographic maps of the Japanese Islands: plate tectonic synthesis from 750 Ma to the present. *Island Arc* **6**, 121–142.

Morris P. A. (1995) Slab melting as an explanation of quaternary volcanism and aseismicity in southwestern Japan. *Geology* **23**, 395–398.

Moyen J. F. (2009) High Sr/Y and La/Yb ratios: the meaning of the 'adakitic signature'. *Lithos* **112**, 556–574.

Mungall J. E. (2002) Roasting the mantle: slab melting and the genesis of major Au and Au-rich Cu deposits. *Geology* **30**, 915–918.

Nakamura K., Kato Y., Tamaki K. and Ishii T. (2007) Geochemistry of hydrothermally altered basaltic rocks from the Southwest Indian Ridge near the Rodriguez Triple Junction. *Mar. Geol.* **239**, 125–141.

Niu M. L., Zhu G., Liu G. S., W D. X. and Song C. Z. (2002) Tectonic setting and deep processes of Mesozoic magmatism in the Middle-south segment of the Tan-Lu fault [J]. *Chinese J. Geol.* **37**, 393–404 (in Chinese with English abstract).

Oyarzun R., Márquez A., Lillo J., López I. and Rivera S. (2001) Giant versus small porphyry copper deposits of Cenozoic age in northern Chile: adakitic versus normal calc-alkaline magmatism. *Miner. Dep.* **36**, 794–798.

Pan Y. M. and Dong P. (1999) The lower Changjiang (Yangzi/Yangtze River) metallogenic belt, east central China: intrusion- and wall rock-hosted Cu–Fe–Au, Mo, Zn, Pb, Ag deposits. *Ore Geol. Rev.* **15**, 177–242.

Pertermann M. and Hirschmann M. M. (2003) Anhydrous partial melting experiments on MORB-like eclogite: phase relations, phase compositions and mineral-melt partitioning of major elements at 2–3 GPa. *J. Petrol.* **44**, 2173–2201.

Petford N. and Atherton M. (1996) Na-rich partial melts from newly underplated basaltic crust: the Cordillera Blanca batholith. *Peru. J. Petrol.* **37**, 1491–1521.

Plank T. and Langmuir C. H. (1998) The chemical composition of subducting sediment: implications for the crust and mantle. *Chem. Geol.* **145**, 325–394.

Prouteau G., Scaillet B., Pichavant M. and Maury R. (2001) Evidence for mantle metasomatism by hydrous silicic melts derived from subducted oceanic crust. *Nature* **40**, 197–200.

Puig A., Herve M., Suarez M. and Saunders A. D. (1984) Calc-alkaline and alkaline miocene and calc-alkaline recent volcanism in the southernmost Patagonian cordillera. *Chile. J. Volcano. Geotherm. Res.* **20**, 149–163.

Rae A. J., Cooke D. R., Phillips D. and Zaide-Delfin M. (2004) The nature of magmatism at Palinpinon geothermal field, Negros Island, Philippines: Implications for geothermal activity and regional tectonics. *J. Volcano. Geotherm. Res.* **129**, 321–342.

Rapp R. P., Watson E. B. and Miller C. F. (1991) Partial melting of amphibolite/eclogite and the origin of Archean trondhjemites and tonalite. *Precambrian Res.* **51**, 1–25.

Rapp R. P. and Watson E. B. (1995) Dehydration melting of metabasalt at 8–32 kbar: implications for continental growth and crust-mantle recycling. *J. Petrol.* **36**, 891–931.

Rapp R. P., Shimizu N., Norman M. D. and Applegate G. S. (1999) Reaction between slab-derived melts and peridotite in the mantle wedge: experimental constraints at 3.8 GPa. *Chem. Geol.* **160**, 335–356.

Rudnick R. L. and Gao S. (2003) Composition of the continental crust. In *In the Crust (ed. R.L. Rudnick) 3 Treatise on Geochemistry* (eds. H. D. Holland and K. K. Turekian). Elsevier-Pergamon, Oxford, pp. 1–64.

Sajona F. G. and Maury R. C. (1998) Association of adakites with gold and copper mineralization in the Philippines. *C.R. Acad. Sci. IIA Earth Planet. Sci.* **326**, 27–34.

Schiano P., Ciocchiatti R., Shimizu N., Maury R. C., Jochum K. P. and Hofmann A. W. (1995) Hydrous, silica-rich melts in the sub-arc mantle and their relationship with erupted arc lavas. *Nature* **377**, 595–600.

Sen C. and Dunn T. (1994) Dehydration melting of a basaltic composition amphibolite at 1.5 and 2.0 GPa: implications for the origin of adakites. *Contrib. Mineral. Petrol.* **117**, 394–409.

Stern C. R. and Kilian R. (1996) Role of the subducted slab, mantle wedge and continental crust in the generation of adakites from the Austral Volcanic Zone. *Contrib. Mineral. Petrol.* **123**, 263–281.

Sun, S.-S. and McDonough, W. F. (1989) Chemical and isotopic systematics of oceanic basalts: implications for mantle composition and processes. In *Magmatism in the Ocean Basins* (eds. A. D. Saunders and M. J. Norry (Eds.)), **42**, 313–345.

Sun W. D., Xie Z., Chen J. F., Zhang X., Chai Z. F., Du A. D., Zhao J. S., Zhang C. H. and Zhou T. F. (2003) Os–Os dating of copper and molybdenum deposits along the middle and lower reaches of the Yangtze River. *China. Econ. Geol.* **98**, 175–180.

Sun W. D., Ding X., Hu Y. and Li X. (2007) The golden transformation of the Cretaceous plate subduction in the West Pacific. *Earth Planet. Sci. Lett.* **262**, 533–542.

Sun W. D., Ling M. X., Yang X. Y., Fan W. M., Ding X. and Liang H. Y. (2010) Ridge subduction and porphyry copper gold mineralization: an overview. *Sci. China Earth Sci.* **2**, 127–137.

Taylor S. R. and McLennan S. M. (1985) *The Continental Crust: Its Composition and Evolution*. Blackwell Scientific Publications, Oxford, 100 pp.

Thiéblemont, D., Stein, G. and Lescuyer, J. L. (1997) Gisements épithermaux et porphyriques: La connexion adakite. Académie de Sciences Paris, Comptes Rendus, **325**, 103–109.

Wang Q., Zhao Z. H., Xiong X. L. and Xu J. F. (2001) Melting of the underplated basaltic lower crust: evidence from Shaxi adakitic sodic quartz dirorite-porphyrites, Anhui province, China. *Geochimica* **30**, 353–362 (in Chinese with English abstract).

Wang Q., Zhao Z. H., Xu J. F., Li X. H., Bao Z. W., Xiong X. L. and Liu Y. M. (2002) Petrology and metallogenesis of the Yanshanian adakite-like rocks in the Eastern Yangtze Block. *Sci. China Ser D.* **32**, 127–136 (in Chinese).

Wang Q., Xu J. F., Zhao Z. H., Xiong X. L. and Bao Z. W. (2003) Petrogenesis of the Mesozoic intrusion rocks in the Tongling Area, Anhui Province, China and constraint to Geodynamics process. *Sci. China Ser D.* **46**, 801–815.

Wang Q., Xu J. F., Zhao Z. H., Bao Z. W., Xu W. and Xiong X. L. (2004a) Cretaceous high-potassium intrusive rocks in the Yueshan-Hongzhen area of east China: adakites in an extensional tectonic regime within a continent. *Geochem. J.* **38**, 417–434.

Wang Q., Zhao Z. H., Xu J. F., Bai Z. H., Wang J. X. and Liu C. X. (2004b) The geochemical comparison between the Tongshankou and Yinzu adakitic intrusive rocks in southeastern Hubei: (delaminated) lower crustal melting and the genesis of porphyry copper deposit. *Acta Petrol. Sinica.* **20**, 351–360.

Wang Q., Wyman D. A., Xu J. F., Zhao Z. H., Jian P., Xiong X. L., Bao Z. W., Li C. F. and Bai Z. H. (2006) Petrogenesis of Cretaceous adakitic and shoshonitic igneous rocks in the Luzong area, Anhui Province (eastern China): Implications for geodynamics and Cu–Au mineralization. *Lithos* **89**, 424–446.

Wang Q., Wyman D. A., Xu J. F., Zhao Z. H., Jian P. and Zi F. (2007a) Partial melting of thickened or delaminated lower crust in the middle of eastern China: implications for Cu–Au mineralization. *J. Geol.* **115**, 149–161.

Wang Q., Wyman D. A. and Xu J. F., et al. (2007b) Early Cretaceous adakitic granites in the Northern Dabie Complex, central China: implications for partial melting and delamination of thickened lower crust. *Geochim. Cosmochim. Acta* **71**, 2609–2636.

Wang Y. (2006) The onset of the Tan-Lu fault movement in eastern China: constraints from zircon (SHRIMP) and $^{40}Ar/^{39}Ar$ dating. *Terra Nova.* **18**, 423–431.

Wang Y. J., Fan W. M., Peng T. P., Zhang H. F. and Guo F. (2005) Nature of the mesozoic lithospheric mantle and tectonic decoupling beneath the Dabie orogen, Central China: evidence from $^{40}Ar/^{39}Ar$ geochronology, elemental and Sr–Nd–Pb isotopic compositions of early Cretaceous mafic igneous rocks. *Chem. Geol.* **220**, 165–189.

Wang Y. L., Wang Y., Zhang Q., Jia X. Q. and Han S. (2004) The geochemical characteristics of Mesozoic intermediate-acid intrusives of the Tongling area and its metallogenesis–geodynamic implications. *Acta Petrol. Sinica.* **20**, 325–338.

Winther K. T. and Newton R. C. (1991) Experimental melting of hydrous low-K tholeiite: evidence on the origin of Archaean cratons. *Bull. Geol. Soc. Denmark* **39**, 213–228.

Wolf M. B. and Wyllie P. J. (1994) Dehydration-melting of amphibolite at 10 kbar: the effects of temperature and time. *Contrib. Mineral. Petrol.* **115**, 369–383.

Xia Q. K., Yang X. Z., Deloule E., Sheng Y. M. and Hao Y. T. (2006) Water in the lower crustal granulite xenoliths from Nushan, SE China. *J. Geophys. Res.* **111**, B11202. doi:10.1029/2006JB004296.

Xie G. Q., Mao J. W. and Li R. L., et al. (2006) SHRIMP zircon U–Pb dating for volcanic rocks of the Dasi formation in southeast Hubei Province, middle-lower reaches of the Yangtze River and its implications. *Chin. Sci. Bull.* **51**, 3000–3009.

Xie G. Q., Mao J. W., Li R. L., Qu W. J., Pirajno F. and Du A. D. (2007) Re–Os molybdenite and Ar–Ar phlogopite dating of Cu–Fe–Au–Mo (W) deposits in southeastern Hubei. *China Mineral. Petrol.* **90**, 249–270.

Xie G. Q., Mao J. W., Li R. L. and Frank P. B. (2008) Geochemistry and Nd–Sr isotopic studies of late mesozoic granitoids in the southeastern Hubei Province, middle-lower Yangtze River belt, Eastern China: petrogenesis and tectonic setting. *Lithos* **104**, 216–230.

Xie J. C., Yang X. Y., Sun W. D., Du J. G., Xu W., Wu L. B., Wang K. Y. and Du X. W. (2009) Geochronological and geochemical constraints on formation of the Tongling meta deposits, middle Yangtze metallogenic belt, east-central China. *Int. Geol. Rev.* **51**, 388–421.

Xing F. M. (1999) The magmatic metallogenetic belt around the Yangtze River in Anhui. *Geol. Anhui.* **9**, 272–279 (in Chinese with English abstract).

Xiong X. L., Xia B., Xu J. F., Niu H. C. and Xiao W. S. (2006) Na depletion in modern adakites via melt/rock reaction within the sub-arc mantle. *Chem. Geol.* **229**, 273–292.

Xu J. F., Shinjo R., Defant M. J., Wang Q. and Rapp R. P. (2002) Origin of Mesozoic adakitic intrusive rocks in the Ningzhen area of east China: partial melting of delaminated lower continental crust? *Geology* **30**, 1111–1114.

Yan J., Chen J. F. and Xu X. S. (2008) Geochemistry of Cretaceous mafic rocks from the Lower Yangtze region, eastern China: characteristics and evolution of the lithospheric mantle. *J. Asian Earth Sci.* **33**, 177–193.

Yan J., Liu H. Q., Song C. Z., Xu X. S., An Y. J., Liu J. and Dai L. Q. (2009) Zircon U–Pb geochronology of the volcanic rocks from Fanchang–Ningwu volcanic basins in the lower Yangtze region and its geological implications. *Chin. Sci. Bull.* **54**, 1–10.

Yang W. and Li S. G. (2008) Geochronology and geochemistry of the Mesozoic volcanic rocks in Western Liaoning: Implications for lithospheric thinning of the North China Craton. *Lithos* **102**, 88–117.

Yang X. Z., Xia Q. K., Deloule E., Dallai L., Fan Q. C. and Feng Min (2008) Water in minerals of the continental lithospheric mantle and overlying lower crust: a comparative study of peridotite and granulite xenoliths from the North China Craton. *Chem. Geol.* **256**, 33–45.

Zhang Q., Wang Y., Qian Q., Yang J. H., Wang Y. L., Zhao T. P. and Guo G. J. (2001) The characteristics and tectonic-metallogenic significances of the adakites in Yanshan period from eastern China. *Acta Petrol. Sinica.* **17**, 236–244.

Zhang Q., Jian P. and Liu D. Y., et al. (2003) SHRIMP dating of volcanic rocks from Ningwu area and its geological implications. *Sci. China Ser. D* **46**, 830–837.

Zhao H. J., Mao J. W., Xiang J. F., Zhou Z. H., Wei K. T. and Ke Y. F. (2010) Mineralogy and Sr–Nd–Pb isotopic compositions of quartz diorite in Tonglushan deposit, Hubei Province. *Acta Petrol. Sinica.* **26**, 768–784.

Zi F., Wang Q., Tang G. J., Song B., Xie L. W., Yang Y. H., Liang X. R., Tu X. L. and Liu Y. (2008) SHRIMP U–Pb zircon geochronology and geochemistry of the Guandian pluton in central Aanhui, China: petrogenesis and geodynamic implications. *Geochimica* **37**, 462–480.

Zhu G., Wang Y., Liu G., Niu M., Xie C. and Li C. (2005) $^{40}Ar/^{39}Ar$ dating of strike-slip motion on the Tan-Lu fault zone, East China. *J. Struct. Geol.* **27**, 1379–1398.

Zindler A. and Hart S. (1986) Chemical geodynamics. *Ann. Rev. Earth Pl. Sci.* **14**, 493–571.

*Associate editor*: Richard J. Walker